

Analysis of Structural Electronic and Vibrational Properties of Two Dimensional Silicon Carbide

By

Md. Rasidul Islam

A thesis submitted in partial fulfillment of the requirements for the degree of Master of Science in Engineering in the Department of Electrical and Electronic Engineering



Khulna University of Engineering & Technology
Khulna 920300, Bangladesh

May 2018

Declaration

This is to certify that the thesis work entitled "*Analysis of Structural Electronic and Vibrational Properties of Two Dimensional Silicon Carbide*" has been carried out by *Md. Rasidul Islam* in the *Department of Electrical and Electronic Engineering*, Khulna University of Engineering & Technology, Khulna, Bangladesh. The above thesis work or any part of this work has not been submitted anywhere for the award of any degree or diploma.

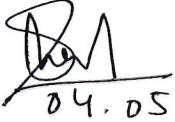


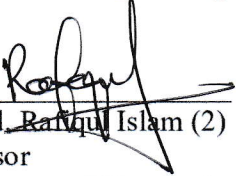
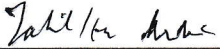
Signature of Supervisor

Signature of Candidate

Approval

This is to certify that the thesis work submitted by *Md. Rasidul Islam* entitled "*Analysis of Structural Electronic and Vibrational Properties of Two Dimensional Silicon Carbide*" has been approved by the board of examiners for the partial fulfillment of the requirements for the degree of *M.Sc. Engineering* in the Department of *Electrical and Electronic Engineering*, Khulna University of Engineering & Technology, Khulna, Bangladesh in May 2018.

BOARD OF EXAMINERS

1. 
04.05.2018
Chairman
(Supervisor)
Dr. Md. Sherajul Islam
Associate Professor
Department of Electrical and Electronic Engineering
Khulna University of Engineering & Technology
2. 
Head of the Department
Department of Electrical and Electronic Engineering
Khulna University of Engineering & Technology
Member
3. 
Dr. Ashraful Ghani Bhuiyan
Professor
Department of Electrical and Electronic Engineering
Khulna University of Engineering & Technology
Member
4. 
Dr. Md. Rafiqul Islam (2)
Professor
Department of Electrical and Electronic Engineering
Khulna University of Engineering & Technology
Member
5. 
Dr. Zahid Hasan Mahmood
Professor
Department of Electrical and Electronic Engineering
Dhaka University, Dhaka, Bangladesh
Member
(External)

Acknowledgement

All approvals belong to the Almighty ALLAH, the most kind hearted and bounteous to all His creatures and their actions. I humbly praise and grateful to Him, Who permits me to live and accomplish tasks including the research work being presented in this thesis.


The author gratefully expresses his deepest sense of gratitude and profound indebtedness to his thesis supervisor, **Dr. Md. Sherajul Islam**, Associate Professor, Department of Electrical and Electronic Engineering (EEE), Khulna University of Engineering & Technology (KUET), Bangladesh, for his continuous supervision, encouragements, precious guidance, advices and helps, constructive criticisms and keen interests throughout the progress of the work. The author believes that work with him is a grand opportunity and would be a never-ending memory.

Last but not least, the author solemnly acknowledges his parents and all the family members, who gave him the utmost mental and financial supports throughout his whole student life and make a way to build up his career in the field of EEE.

Abstract

Two dimensional silicon carbide (2D-SiC) has fascinated incredible research attention recently because of its large direct bandgap and high exciton binding energy. Nonetheless, no well-established researches have been performed on 2D-SiC combining its physical, electronic and vibrational properties. Here, we have investigated the details of the full physical picture of novel 2D-SiC describing their structures and functions as well as the electronic tunability and phonon properties using the first principle density functional theory. The structural properties show that 2D-SiC has the honeycomb graphene like structure with lattice constant 5.72 Ry (3.101 Å). The positive phonon modes in the vibrational properties indicate that the plane structure of 2D-SiC is dynamically stable. The calculated projected density of states (PDOSs) have exposed that the conduction and valence band edges at the K point have been constructed by the π and π^* -bands, which are formed due to the bonding and anti-bonding combination of Si-3p_z and C-2p_z orbitals.

The electronic properties of semiconductor materials are greatly influenced by the spin orbit coupling (SOC) effect. The effects of SOC on the electronic structure of 2D-SiC have been studied using the first-principle calculation which is implemented on quantum espresso 6.1 version. Though the electronic band structure shows that the 2D-SiC monolayer possesses a direct band gap of 2.71 eV, the electronic band become split and the band gap turns to 2.827 eV while considering the SOC effect. It is found that SOC induces splitting in both valence and conduction bands of this material. A SOC induced bandgap on the order of 117 meV has been generated at the *K*-point. The calculated partial electron density of state exposes that the silicon 3p electrons and carbon 2p electrons are critical in forming the electronic bandgap. Phonon density of states, thermal properties, Raman and Infrared spectra of this material have been also calculated. In addition, the effect of Si and C vacancies on the electronic properties of 2D-SiC has been addressed with and without considering SOC effect. These findings suggest that the monolayer 2D-SiC may present a new platform of 2D materials, with a rich variety of properties for applications in electronics, optoelectronics and spintronics devices.

Dedicated
To
My Beloved Parents

Respected Teachers

Contents

	PAGE
Title Page	i
Declaration	ii
Certificate of Research	iii
Acknowledgement	iv
Abstract	v-vi
Dedication	vii
Contents	viii-ix
List of Figures	x-xi
List of Illustrations	xii
Nomenclature	xiii
CHAPTER I Introduction and Research Objectives	1
1.1 Introduction	2
1.2 Motivation	4
1.3 Objectives	6
1.4 Synopsis of Dissertation	7
CHAPTER II Fundamentals of SiC	9
2.1 Introduction	10
2.2 History of SiC	10
2.3 Physical properties of SiC	11
2.4 2D Structure from bulk structure	14
2.5 Graphene	15
2.6 Two Dimensional (2D) SiC ₂	17
2.7 Two Dimensional (2D) SiC ₇	19
2.8 Two Dimensional (2D) SiC	20
2.9	
CHAPTER III Theoretical Background	22
3.1 Introduction	23
3.2 Schrödinger equation and its Hamiltonian	23
3.3 Born-Oppenheimer approximation	24
3.4 The Hartree approximation	25
3.5 The Hartree-Fock approximation	26
3.6 The correlation energy	27
3.7 The Hohenberg-Kohn theorems	27
3.8 The exchange-correlation approximations	28
3.9 The Kohn-Sham theorem	29
3.10 Pseudopotential	31

3.11	Spin-Orbit coupling effect	33
3.12	Phonon properties	34
3.13	Thermal properties	35
3.14	Quantum Espresso	36
3.15	Computational details	37
CHAPTER IV	Results and Discussions	41
4.1	Introduction	41
4.2	Structural properties	41
4.3	Electronic properties without SOC effect	42
4.4	Electronic properties with SOC effect	44
4.5	Phonon properties	46
4.6	Raman and infrared (IR) spectroscopy	47
4.7	Thermal properties	48
4.8	Effect of vacancy defects on 2D-SiC	49
4.8.1	Carbon and silicon vacancy effects on electronic properties	52
4.8.2	Combined vacancy and SOC effects on electronic properties	55
CHAPTER V	Summary and Outlook	56
5.1	Conclusion	57
5.2	Future Work	58
	Bibliography	59
	Appendix Quantum Espresso coding for scf calculation	66
	List of publications	67

LIST OF FIGURE

Figure No	Description	Page
1.1	Some major application of SiC in different devices	2
1.2	Market trend of SiC power devices using data compiled by Rohm, based on Fuji Keizai Reality and Future Prospect of Next Generation Power Device and Power Electronics	3
2.1	Stick and ball models of 3C and pH ($p = 2, 4, 6$) polytypes. Cations: red spheres, anions: blue dots. The stacking sequence of the cation–anion bilayers is indicated by the symbols A, B or C. Primitive unit cells are shown for the pH polytypes, while a non-primitive hexagonal cell is depicted to illustrate the cubic 3C symmetry. The primitive basis vectors a_i ($i = 1, 2, 3$) are also shown.	11
2.2	Crystal structure of 4H-SiC. Bond configuration of step-terrace structure on a 4H-SiC (0001) surface viewed from the direction.	12
2.3	(Color online) Optimized atomic structure with relevant structural parameters, corresponding energy band structure and frequencies of phonon modes of 3D bulk SiC in zinc blende and wurtzite structures. Zero of energy of the band structure is set at the Fermi level, and band gap is shaded	13
2.4	Graphene, graphite, single-walled carbon nanotube (SWNT) and C_{60} structures make sp^2 type bonding, whereas diamond makes sp^3 type bonding	16
2.5	Band structure of graphene: (a) Graphene honeycomb lattice. (b) tight-binding band structure of graphene (c) Band structure close to the Dirac Point	17
2.6	(a) Optimized structure of g-SiC ₂ siligraphene with unit cell outlined as red lines. Red vectors: a_1, a_2 : graphene lattice vectors. (b) The band structure of g-SiC ₂ monolayer calculated based on PBE and HSE06. The π bands are marked in red. (c) The total DOS and projected DOS (PDOS) of g-SiC ₂ siligraphene. The Fermi energy is set as zero.	18
2.7	(a) The optimized structure of g-SiC ₇ siligraphene. (b) Band structure	19

of g-SiC7 siligraphene based on GGA-PBE (left panel) & HSE06 (right panel) calculations, respectively. Fermi level is set as zero (c) Projected density of states (PDOS) of g-SiC7 siligraphene.

2.8	Unit cell and lattice vectors of planar honeycomb SiC	21
3.1	Flowchart of Kohn-Sham Theorem.	30
3.2	Schematic for the calculation of electronic properties of novel 2D SiC	39
3.3	Schematic for the calculation of phonon properties of novel 2D-SiC	39
4.1	Optimized atomistic model of 2D-SiC with unit cell outlined as dashed line. (b) The corresponding first Brillouin zone and high symmetry points	41
4.2	Total energy per unit cell of 2D-SiC with the variation of (a) lattice constant (b) kinetic energy cut-off and (c) <i>K</i> -points	42
4.3	Electronic band structure and (b) density of states (DOS) of 2D-SiC without considering the SOC. The Fermi level is set to zero. A direct energy band gap at <i>K</i> -point is shown by the red arrow	43
4.4	Projected density of state (PDOS) of 2D-SiC with separate contributions from each orbital atoms without SOC.	44
4.5	(a) Electronic band structure and (b) DOS of 2D-SiC with SOC. The band structure changes and increases the energy gap at the <i>K</i> -point due to the SOC effect	45
4.6	PDOS of 2D-SiC with separate contributions from each orbital atoms. The p-orbital splits into two new branches due to the SOC	46
4.7	(a) Phonon dispersion relationship with Ultrasoft pseudopotential using first principle density function theory, and (b) Corresponding Phonon Density of State of 2D-SiC	47
4.8	(a) Raman and (b) IR Spectra of 2D-SiC	49
4.9	The Helmholtz free energy F_A at constant volume of 2D-SiC monolayers are calculated as a function of temperature with harmonic approximation	51
4.10	(a) Atomic structure of 2D-SiC (4×4 supercell), (b) Single carbon	51

	vacancy, and (c) Single silicon vacancy of 2D-SiC (Si is red color and carbon is blue color).	
4.11	(a) Electronic band structure of 2D-SiC (4×4 supercell) using DFT (b) Corresponding density of state (DOS).	52
4.12	(a) Electronic band structure of 2D-SiC with carbon vacancy defect (4×4 supercell), (b) DOS	53
4.13	Electronic band structure of 2D-SiC with silicon vacancy defect (4×4 supercell) (b) DOS	54
4.14	Electronic band structure of 2D-SiC with carbon vacancy defect, including SOC effect.	54
4.15	Electronic band structure of 2D-SiC with silicon vacancy defect, including SOC effect.	55

LIST OF ILLUSTRATION

2D	Two Dimensional
SiC	Silicon Carbide
LED	Light Emitting Diode
SOC	Spin Orbit Coupling
CB	Conduction Band
VB	Valance Band
E_g	Band gap energy (eV)
BZ	Brillouin zone
DOS	Density of State
PDOS	Projected Density of State
IR	Infrared
GHz	Gigahertze
GaAs	Gallium Arsenide
GaN	Gallium Nitride
SWNT	Single-walled carbon nanotube
F_A	Helmholtz free energy
PHDOS	Phonon density of states
eV	Electron volt
meV	mili electron volt
LA	Longitudinal acoustic
LO	Longitudinal optical
ZO	Out of plane optical
TA	Transverse acoustic
TO	Transverse optical
ZA	Out of plane acoustic

NOMENCLATURE

c, a	Lattice parameter (nm)
Ψ	Wave function
T	Temperature (K)
M_i	Nucleus mass
Z_i	Nucleus charge
V_{ext}	Potential energy of the electrons
V_{int}	Coulomb interaction
\hbar	Planck's constant
\hat{p}	Momentum
\hat{H}^{SOC}	Spin-orbit coupling operator

Chapter

I

INTRODUCTION AND RESEARCH OBJECTIVES

Chapter at a Glance

- | | |
|-----------------------------------|--------------------|
| • Introduction | Section 1.1 |
| • Thesis Motivation | Section 1.2 |
| • Objectives | Section 1.3 |
| • Synopsis of Dissertation | Section 1.4 |

1.1 Introduction

In the last decades, Silicon Carbide (SiC), a binary compound of carbon and silicon has appealed tremendous research attention owing to its notable physical properties including high saturation velocity of carriers, high breakdown field, better strength, and good thermal conductivity [1-5]. The SiC is used for the fabrication of electronic devices having a high-temperature, high-frequency, and high-power ratings [6]. Formerly, many devices encompassing super-capacitors, gas detecting system have been fabricated using SiC [7-8]. Due to its unique properties, SiC based devices can be used in severe conditions, in particular eminent temperature, oxidized and corrosive atmosphere [9-11]. The wide tunable bandgap (2.3-3.4 eV) of SiC also promises its extensive applications in optoelectronics of visible and ultraviolet range [12-13]. The SiC in different devices application has already been used in the last era is shown in Fig. 1.1. It is forecasted that the major parts of power electronics devices will be replaced by SiC within 2020 which shown in Fig. 1.2.

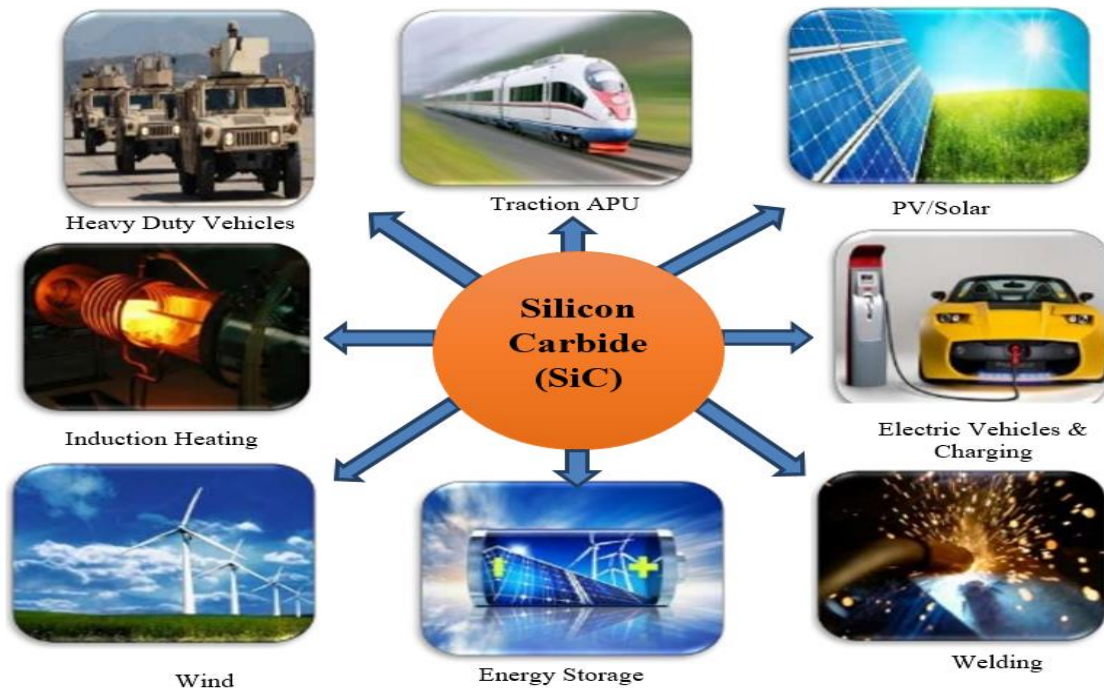


Fig. 1.1: Some major application of SiC in different devices [15].

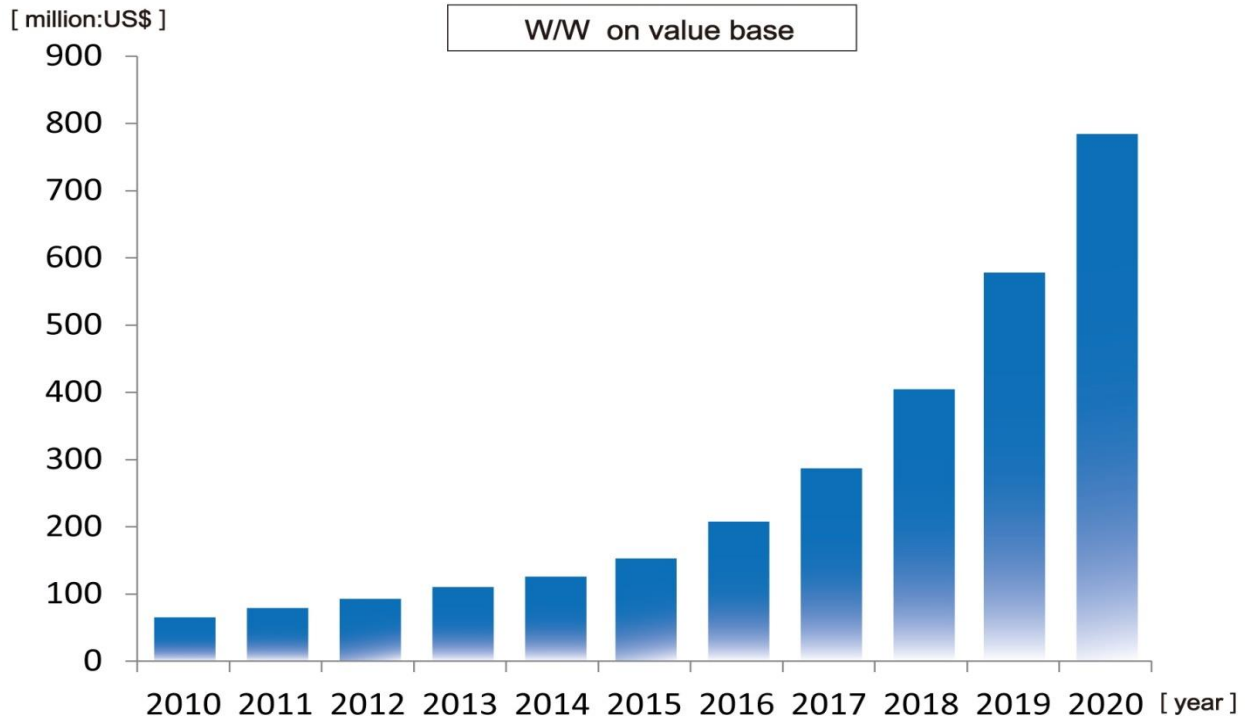


Fig. 1.2: Market trend of SiC power devices using data compiled by Rohm, based on Fuji Keizai Reality and Future Prospect of Next Generation Power Device and Power Electronics [19].

In the 1950s, Schockley predicted that SiC would quickly replace Si because of its superior properties. Generally, the critical electrical field of bulk SiC is higher than that of Si, which makes SiC an excellent choice for power semiconductor devices [16]. SiC has a thermal conductivity about three times higher than that of silicon. Therefore, heat dissipation by the losses can be conducted from within the semiconductor with a much lower temperature drop across the semiconductor material. Because of its high melting temperature, the SiC device can operate well over 400°C much higher than the maximum allowable junction temperature of standard silicon technology 150°C [17]. This property results in significant cost reduction of the cooling system since less expensive cooling materials and methods can be used. The SiC devices have larger current density than the maximum current density of silicon devices [18]. This property will reduce cost and will, over time, help to offset some of the cost disadvantages of the SiC device. These promising features of SiC predict that, Si will rapidly be switched by SiC. However, bulk SiC is a typical sphalerite or a wurtzite compound semiconductor with more than 250 alloy types [14], which have different band gaps and diverse physical properties. Among the

alloy of the bulk SiC, it has six commonly used stacking configurations represented as 3C (zinc blende), 2H (wurtzite), 4H, 6H, 15R and 21R [15]. Thus, the goal of SiC based electronics is greatly hindered.

The synthesis of graphene by Novoselov et. al. [21] has initiated the immense study of other new two-dimensional (2D) materials with novel physical properties. 2D materials possess unique electrical, mechanical, chemical and optical properties due to their thickness dependent surface and quantum confinement effects [20]. Although mono-layer graphene sheet shows exceptional electronic properties such as extremely high carrier mobility and the long mean-free path, the zero bandgap associated with Dirac fermions hinders its application in electronic devices. Recent theoretical studies have shown that Bulk SiC can be transformed into a 2D stable mono-layer honeycomb structure similar to graphene [21]. 2D-SiC has appealed tremendous research attention because of its large direct gap along with a high exciton binding energy [22]. These intriguing properties are very much advantageous for optoelectronic device applications, such as light emitting diodes (LEDs) or solar cells [23]. By analogy with Cu_2O , the high exciton binding energy in the 2D-SiC structure may induce the Bose–Einstein condensate effect [24]. Mono layer SiC also exhibits enhanced photoluminescence than its bulk counterparts. 2D-SiC, in particular, is of special interest, as it is speculated to show such properties that their sphalerite or wurtzite counterparts may not have. Moreover, 2D-SiC inherits more robust structure than graphene. The formation of quasi 2D-SiC has also been reported by atomic resolution scanning transmission electron microscopy [25]. Therefore, 2D-SiC is expected to be a promising semiconductor fascinating to both fundamental research and wide applications in electronic and optoelectronic devices. Although 2D SiC is predicted to have the potentials for wide applications in nano and optoelectronic devices due its superior properties, the theoretical studies on the 2D-SiC system are just limited to several scattered results only [26-27]. A detailed understanding of full physical picture of 2D-SiC describing their structures and functions as well as the electronic tenability and phonon properties are urgently needed for practical applications.

1.2 Motivation

Because of interesting electronics, mechanical and thermal properties it possesses, bulk SiC drew attention of both scientists and device engineers for past years. Nanotechnology not only aims to reduce well known technology to nanoscale but also tries to explore the new application areas,

taking advantage of the quantum world. While the two-dimensional structure of semiconductors has a subject of active study leading to the optoelectronics devices, 2D-SiC is a great research interest for device application. Two-dimensional graphene-like 2D-SiC has emerged as an intriguing new class of layered nanostructure. Recently, Shi and co-workers reported the stability and electronic properties of 2D $\text{Si}_x\text{C}_{1-x}$ ($0 < x < 1$) [28] monolayers mixing carbon and silicon atoms. They found that stoichiometry and bonding structure of the 2D-SiC monolayers can greatly affect the electronic properties [29]. For example, with the same stoichiometry, pt-SiC₂ is metallic but g-SiC₂ is a semiconductor due to their different bonding structures. From graphene to 2D-SiC, the band gap of siligraphene can vary in the range of 0–3 eV, independent of the increasing content of silicon. The g-SiC₂ has exhibited great potential as a novel donor material in excitonic solar cells. And another siligraphene, g-SiC₃ can serve as a topological insulator (TI) superior to graphene [29]. However, the theoretical studies on 2D-SiC system are just limited to several scattered results only.

On the other hand, electronic properties of semiconductor materials and topological insulators are greatly affected by the spin orbit coupling (SOC) [30]. Though in light constituent elements show the weak SOC, the strong SOC effect is observed in heavier atoms. Due to the breaking of the inversion symmetry from bulk structure to the monolayer structure, the SOC effects are unpredictably large. The SOC is produced by the orientation of electron spins and orbital motion of electrons which might be originated due to the relativistic effect. Generally, the valence band edge is created by p-orbital state and the conduction band is created by s-orbital state for most of the semiconductors. A degenerate p-orbital split state is produced and s-orbital state remains unchanged owing to the SOC [31]. In the presence of SOC, an energy gap between the spin-split states is created. The SOC induced bandgap promotes the quantum spin Hall Effect [32], which makes the crystal a topological state. This peculiar behavior gives rise to potential uses in dissipation less electronics and spintronic devices.

The electronic band structure of graphene has a zero bandgap near the Fermi level at the K and K_0 points in the Brillouin zone (BZ), which means the low-energy dynamics of electrons in graphene near these Dirac points is comparable to that of relativistic Fermions [32]. There is no SOC effect because of $2s$ and $2p$ orbitals different quantum numbers of a single carbon atom, however, among the $2p$ orbital the SOC effect is present. The bandgap can open at the Dirac

points due to including the SOC and change the ideal representation of observing relativistic Dirac particles in graphene. Literature [33] shows that a small bandgap of $\sim 1 \mu\text{eV}$ is created while considering the intrinsic SOC in graphene. The SOC induces a bandgap of $\sim 1.6 \text{ meV}$ [34] in Si counterpart 2D structure so called the silicene, much greater than that of graphene. Compared to graphene and silicene 2D structures, the SOC effect on monolayer SiC is more interesting because strong spin orbital interaction is expected for this material. However, an in-depth understanding of the effect of SOC in 2D-SiC remains scarce. Therefore, studying the SOC effect on the electronic properties in 2D-SiC is one of the major issues for its prospective applications.

Besides the different properties, vacancy defect is the important parameter for device application. The presence of defects definitely changes and modifies a material's fundamental properties. Any kind of defect concentrations has a significant effect on mechanical strength, optical absorption, electronic and thermal transport properties of a material. Especially defects play a vital role in low-dimensional systems. Due to quantum confinement, defects have a dominating effect on physical properties of low dimensional materials. It has been shown that the vacancy defects have remarkable effects on 2D graphene honeycomb structure and its nanoribbons [35-36]. The modification of electronic and magnetic properties of graphene sheets or nanoribbons has been happened due to vacancy defects. We expect that similar effect of vacancy defects can occur in the electronic properties of the 2D-SiC honeycomb structure. Despite the significance of SOC and vacancy defects for monolayer 2D-SiC systems, to the best of our knowledge, thus far no study has been conducted on the SOC effect on the electronic structure of defective 2D-SiC. Therefore, an intuitive insight on how the defects change the structural and electronic properties of this material is indispensable for promising technological applications.

1.3 Aims and objectives

Motivated by the fabrication of graphene and other 2D materials as well as the extraordinary physical properties for the exciting applications of optoelectronic devices in the imminent future, the structural, electronic and vibrational properties of 2D-SiC have been investigated thoroughly. The electronic properties of semiconductor materials are greatly influenced by the SOC effect. Therefore, due to the presence of SOC in 2D-SiC the electronic properties have been changed.

Besides, the different properties, the electronic properties have also modified due to vacancy defects. To quantify the electronic properties including the vacancy defect and SOC effect is very important objectives of this dissertation. The main objectives of this dissertation have been spun in the following headings:

- I To determine energetically favored structures and dynamic stability to get minimum energy of 2D-SiC using energy variation with respect to the lattice constant, kinetic energy and K-points.
- II To extract the vibrational properties to check the dynamical stability and calculate the thermal properties, Raman spectroscopy and infrared spectroscopy of 2D-SiC.
- III To calculate the electronic properties such as band structure, density of state and projected density of state of 2D-SiC.
- IV To study spin orbit coupling effect on the electronic properties of 2D-SiC.
- V To study the effect of vacancy type defects like a single carbon and silicon vacancy on the electronic properties of 2D-SiC with and without considering SOC.

1.4 Synopsis of Dissertation

The thesis is organized as follows:

Chapter 2 summarizes the basic properties of bulk SiC. It also describes the properties of different types of two dimensional (2D) honeycomb structures, including 2D-SiC honeycomb structure.

Chapter 3 focuses on the theoretical background and approximation methods. It also introduces the used computational technique, which allows calculating the different properties of 2D-SiC. After the motivation for the use of the first principle density functional theory, its details simulation procedures and validity is explained.

In Chapter 4, our studies and results are presented. The structural, electronic and vibrational properties of 2D-SiC have been calculated using Kohn-Sham theorem. Including the SOC effect

on the electronic properties have also calculated. It has also calculated the electronic properties with silicon and carbon vacancy of 2D-SiC structure.

Finally, In Chapter 5, a brief conclusion summarizes the result of our studies, combined with an outlook on possible future research directions.

Chapter

II

Fundamentals of Silicon Carbide

Chapter at a Glance

- | | |
|---|--------------------|
| • Introduction | Section 2.1 |
| • History of SiC | Section 2.2 |
| • Physical properties of SiC | Section 2.3 |
| • 2D Structure from bulk structure | Section 2.4 |
| • Graphene | Section 2.5 |
| • Two Dimensional (2D) SiC₂ | Section 2.6 |
| • Two Dimensional (2D) SiC₇ | Section 2.7 |
| • Two Dimensional (2D) SiC | Section 2.8 |

2.1 Introduction

This chapter is intended to provide an introduction and overview of the fundamental concepts of bulk silicon carbide. It also provides overview of the graphene and related two dimensional materials, especially, for the two dimensional silicon carbide.

2.2 History of SiC

SiC is naturally synthesized in the atmospheres of carbon rich red giant stars and by supernova remnants. No natural crystals can be found on Earth and therefore SiC never attracted man's interest as other crystals like diamond did. Jon's Jacob Berzelius, also known for his discovery of silicon, was most probably the first to synthesize SiC. He published in 1824 a paper in which he assumed there was a chemical bond between silicon and carbon in one of the samples he had produced [37]. But it was not before 1892 that SiC came into focus as a useful material. E. G. Acheson was looking for a suitable material that could substitute expensive diamonds needed for grinding and cutting purposes. He mixed coke and silica in a furnace and found a crystalline product characterized by great hardness, refract-ability, and infusibility. This product was shown to be a compound of silicon and carbon and was called carborundum [38]. In 1907, H. J. Round produced the first Light Emitting Diode (LED) based on SiC. He reported that "on applying a potential of 10 volts between two points on a crystal of carborundum, the crystal gave out a yellowish light" [39]. In 1912, H. Baumhauer used the word "polytypic" to describe the ability of SiC to crystallize into different forms varying only in their stacking order in one direction. The evolution of SiC as an electronic material then took several decades. In 1955, Lely presented a new method to grow high quality SiC crystals. This triggered the development of SiC as a semiconductor material and SiC became even more popular than Si and Ge.

However, the difficulty in obtaining high-purity SiC wafers and the rapid success of the Si technology caused a drop in the interest in SiC. In 1978, Tairov and Tsvetkov then managed to produce high purity SiC substrates by seeded sublimation growth [40]. The first SiC wafer had been made. Another major step forward was made in 1983 when Nishino, Powell, and Hill realized the first hetero-epitaxy of SiC on Si [41]. In 1987, this technique was further improved and the next stage of SiC evolution started when high-quality hetero-epitaxy was performed at low temperatures on off-axis substrates using "step-controlled epitaxy" [42]. Cree Inc. was

founded the same year and two years later, the company introduces the world's first blue LED and began to sell SiC wafers. Along with better epitaxy, the improvement of the diameter and quality of the wafers continued until the production of 4 inch SiC single crystals was reached in 1999. SiC Schottky diodes and high-frequency Metal Semiconductor Field Effect Transistor (MESFETs) are now commercially produced but research on electronic SiC-based devices is still active in view of many possible applications.

2.3 Physical properties of different SiC structures

SiC is the only known binary compound of silicon and carbon and possesses a one-dimensional polymorphism called polytypic. In a polytypic compound, similar sheets of atoms or symmetrical variants are stacked on top of each other. The differences between the polytypic arise only in the direction perpendicular to the sheets. In SiC, each sheet represents a bilayer of C atoms right a top Si atom. The sheets can be represented as a close-packed array of Si-C units forming a two-dimensional pattern with six-fold symmetry. There are different possibilities for arranging the second sheet on top of the first one in a close-packed configuration.

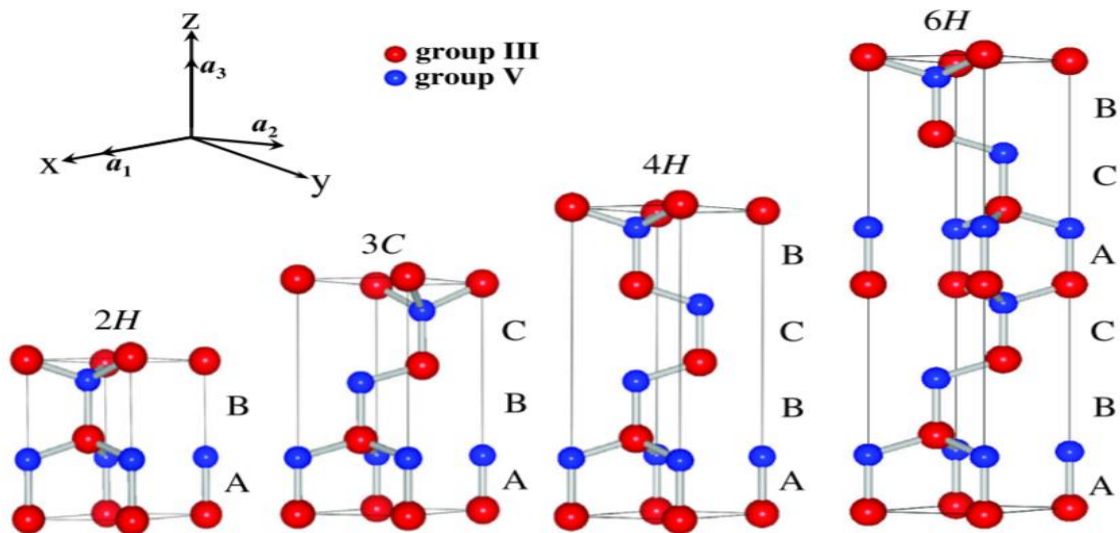


Fig. 2.1: Stick and ball models of 3C and pH ($p = 2, 4, 6$) polytypes. Cations: red spheres, anions: blue dots. The stacking sequence of the cation–anion bilayers is indicated by the symbols A, B or C. Primitive unit cells are shown for the pH polytypes, while a non-primitive hexagonal cell is depicted to illustrate the cubic 3C symmetry. The primitive basis vectors a_i ($i = 1, 2, 3$) are also shown [44].

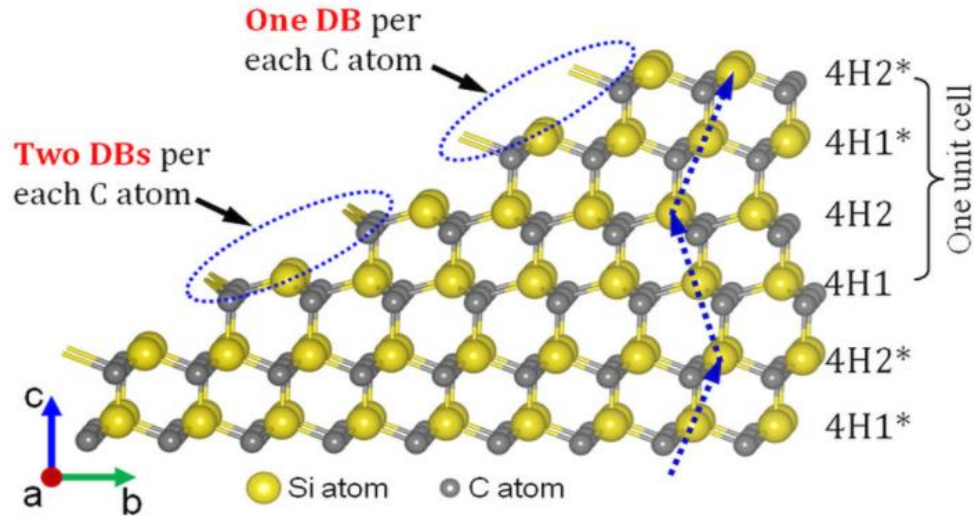


Fig. 2.2: Crystal structure of 4H-SiC. Bond configuration of step-terrace structure on a 4H-SiC (0001) surface viewed from the direction [45].

The second sheet can be displaced along, for example, the direction [1100] until the spheres lie on positions B or along, for example, direction [1100] until the spheres lie on positions C. A close-packed hexagonal plane of spheres centered on points A. A second identical plane can be placed on top of the first one, with the centers of spheres over either points B or C [43]. The stacking orders are illustrated for zinc blende and three hexagonal crystal structures in figure 2.2. We call them polytypes because only the stacking in one direction is varied. In the Ramsdell notation [46] the pure cubic zb stacking of cation–anion double layers in the [111] direction is called 3C in order to indicate the periodicity and the Bravais lattice. The pure hexagonal wz stacking in the [0001] direction is denoted with 2H for similar reasons. The two other polytypes displayed in figure 1 represent combinations of cubic (c) and hexagonal (h) bilayers which are distinguished by the same (c) or opposite (h) direction of the cation–anion bonds with a certain angle to the [0001] direction. The four examples in Fig. 2.1 are 2H, 3C, 4H and 6H in Ramsdell notation with four or six double layers and, hence eight or twelve atoms in the corresponding hexagonal unit cell. According to a previous calculation result, the extra energy required to deposit a new layer on a 4H₁ terrace is much higher than that for a 4H₂ terrace [47]. In other words, a 4H₁ terrace is much more stable than a 4H₂ terrace.

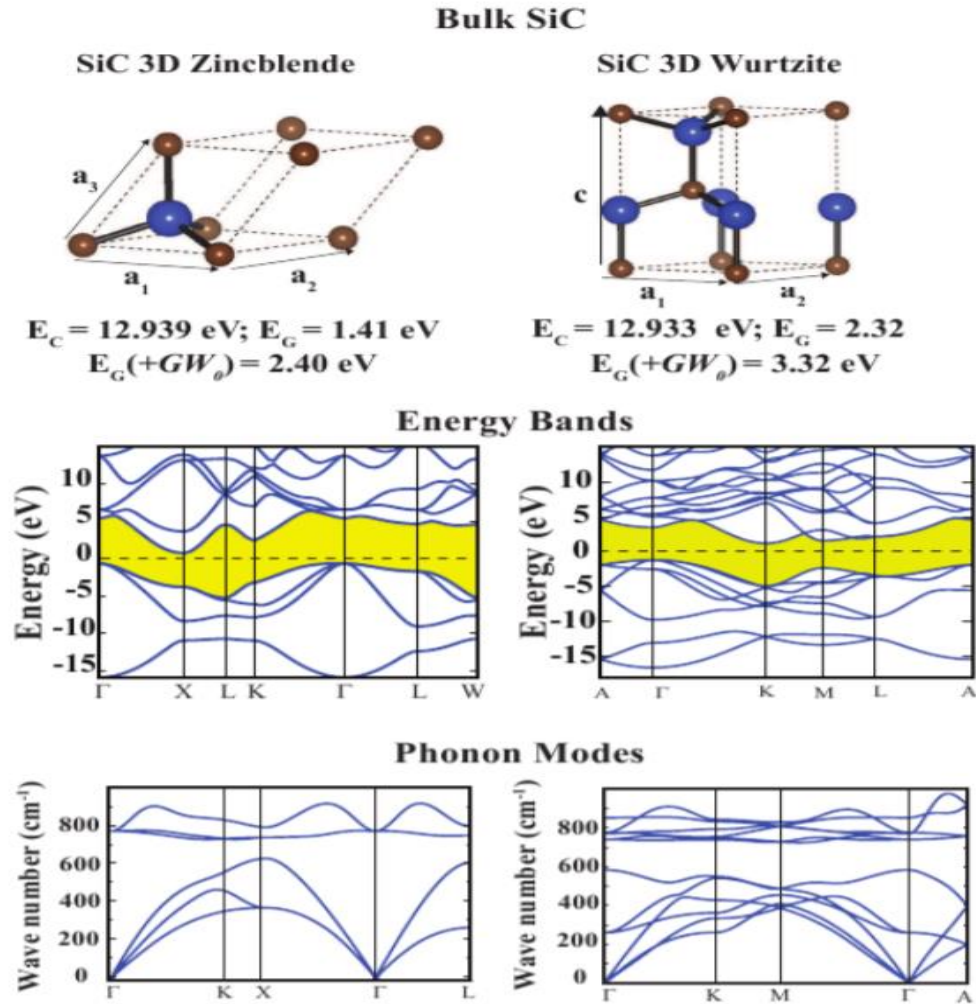


Fig. 2.3: (Color online) Optimized atomic structure with relevant structural parameters, corresponding energy band structure and frequencies of phonon modes of 3D bulk SiC in zinc blende and wurtzite structures. Zero of energy of the band structure is set at the Fermi level, and band gap is shaded [48].

On the basis of this calculation result, Arima *et al.* proposed that the etching rates of $4H_1$ and $4H_2$ terraces are different, resulting in the generation of an a-b type step-terrace structure in a catalyst-referred etching process. However, the difference between $4H_1$ and $4H_2$ terraces cannot explain the generation of a-b-a*-b* type and a-a type step-terrace structures. On the other hand, in the calculation of the extra energy required for deposition, the number of dangling bonds (DBs) at the step edge was not taken into the consideration. More than 250 SiC polytypes have been identified, with some having stacking sequences of several hundreds of bilayers. The

crystal structures of SiC can be cubic, hexagonal or rhombohedral. In the two polytypes particularly suited for electronics, namely 4H- and 6H-SiC. These two polytypes are named according to Ramsdell's notation [48] where the number stands for the periodicity in the stacking direction (i.e. the number of letters A, B, C needed to define the unit cell) and the letter relates to the crystal structure, here H for hexagonal. Following the ABC notation, 4H-SiC has a stacking sequence labeled ABCB and ABCACB for 6H-SiC (Fig. 2.1). According to the notations for a and c for hexagonal crystal structures, the lattice parameter a along the $[1010]$ and 15.11 \AA for 4H-SiC both 4H-SiC and 6H-SiC and c along $[0001]$ is 10.06 \AA and 6H-SiC, respectively [49] for more details on structural parameters). These two hexagonal polytypes share many desirable mechanical, thermal, and electronic properties. SiC comparison to conventional silicon, is an ideal candidate of choice for high-temperature, high-speed, high-frequency, and high-power applications [50]. It has a wide band gap, high thermal conductivity, high saturated electron drift velocity, and high breakdown electric field. SiC is also hard, chemically stable, and resistant to radiation damage. For industrial purposes, SiC can be n-type doped using nitrogen or phosphorus as donors and p-type doped using boron, aluminum or gallium as acceptors. Despite these desirable bulk properties, SiC-based devices are still facing many performance challenges [51].

2.4 2D Structure from bulk structure

Two dimensional materials have been investigated for over 50 years, but since the isolation of graphene in 2004 there has been growing interest in the field. There have been significant improvements in the identification and production of layered materials which opens up a range of applications including heterostructure components and specialized electronic devices [52]. There are several reasons for the growing number of devices being engineered using these materials, but chief amongst them is the control of electronic properties, confinement effects and increased surface areas, all due to reduced dimensionality. Very often the thin film structures lead to flexible devices which have beneficial optical properties, including transparency [53]. The change from bulk graphite to single layer graphene for example, shows the extent to which dimensionality plays a role in electronic behavior. Graphite is semi-metallic with a mobility of roughly $3,000 \text{ cm}^2/\text{Vs}$ at 77 K, whereas in graphene even at room temperature the mobility has been found to be around $10,000 \text{ cm}^2/\text{Vs}$. Much of this is due to the difference in electronic behavior, whilst both are semi-metallic; in single layer graphene the band structure close to the

Fermi level is linear and the electrons are described as massless Dirac fermions [54]. This has in turn led to some relatively unusual phenomena, including a room temperature quantum Hall effect and a minimum level of conductance. This has been matched by mechanical properties that outperform steel and thermal transport properties better than diamond [55]. Graphene has definitely been the single biggest source of the interest and is the most widely used and studied two dimensional materials, but two of the main drawbacks are the lack of a band gap and the need to redesign existing devices to incorporate carbon based electronics and traditional Si-based device architectures. Graphene, the 2D honeycomb structure of carbon has been the source for the inspiration of all other monolayer honeycomb materials. Advances in materials growth and control techniques have made the synthesis of the isolated graphene and its ribbons in different orientations possible. Recent studies on the quasi one dimensional graphene ribbons revealed interesting size and geometry dependent electronic and magnetic properties. What makes carbon atoms stay planar in honeycomb form is the strong coupling of p_z orbitals. Silicon having a larger radius than carbon makes the honeycomb structure by getting slightly buckled (puckered) named silicene [56].

However, graphene and silicene both exhibit zeroes band gaps, making them unsuitable for the controlled and reliable transistor operation, consequently limiting their widespread applications in optoelectronic devices, such as light-emitting diodes, field effect transistors, and solar cells. It is therefore highly desired to open an energy gap in graphene and silicene. But this is a big challenge, because their unique electronic structures originate from the massless Dirac fermion-like behavior of the charge carriers. Intensive studies of 2D nanomaterial's lead to not only successfully syntheses of silicene, SiC, CN, C_3N_4 , BN, ZnO, and MS_2 but also theoretical predictions of some novel compounds, such as B with low-buckled configurations, graphitic GaN–ZnO, boron–carbon compounds, carbon nitride, germanene, pt-SiC₂, GeC, SnC, tetragonal TiC, group III –VI compounds, and MX_2 chalcogenides [57].

2.5 Graphene

Graphene, graphite, carbon nanotubes and fullerenes are categorized in carbon based π electron systems in honeycomb network, which are distinguished from sp^3 -based Nano carbon systems having a tetrahedral network such as diamond. Graphite can be viewed as a stack of graphene layers.

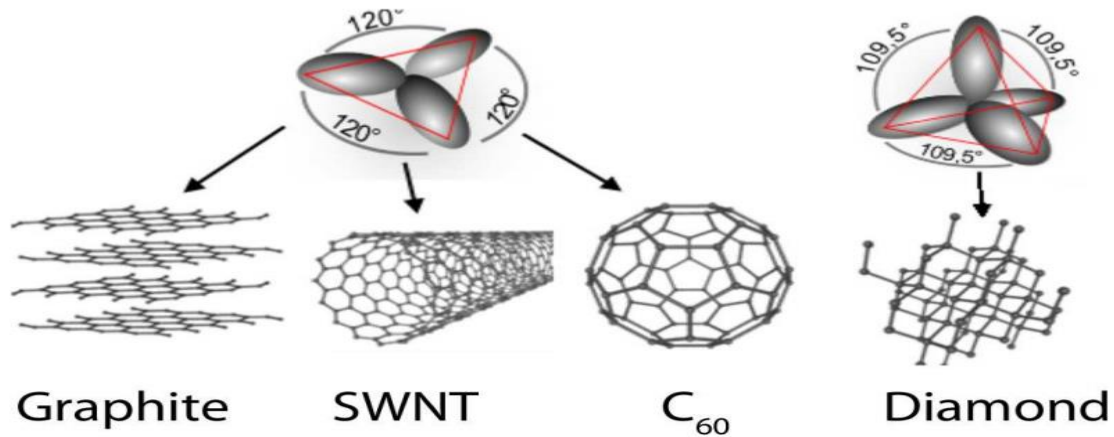


Fig. 2.4: Graphene, graphite, single-walled carbon nanotube (SWNT) and C_{60} structures make sp^2 type bonding, whereas diamond makes sp^3 type bonding [58].

Carbon nanotubes are rolled up cylinders of graphene and fullerenes are the molecules consisting of wrapped graphene by the introduction of pentagons on the hexagonal structure. The diamond is a transparent crystal of tetrahedral bonded carbon atoms and crystallizes into the face centered cubic lattice structure. With the sp^2 hybridization of one s-orbital and two p-orbitals results in a triangular planar structure with a formation of an σ -bond between carbon atoms which are separated by 1.42 Å. The perfect 2D graphene is an infinite network of hexagonal lattice, in contrast to ideal graphene which is a nano sized flat hexagon network with the presence of open actual edges around its periphery. The open edges become important for nanoribbons. An amusing factor about the band structure of graphene is that it has 2D electron system with electrons with zero effective mass. The property has an origin of the unique band structure of graphene, which has linear dispersion relation. Fig. 2.2.4(a) shows the honeycomb lattice of graphene. Each carbon atom is covalent bonded with nearest three carbon atoms through sp^2 hybridization, with carbon-carbon bond length of $a_0=0.142\text{nm}$. The structure can be seen as a triangular lattice with a basis of two atoms per unit cell, which is represented by a_1 and a_2 :

$$\mathbf{a}_1 = \frac{a}{2}(3, \sqrt{3}), \mathbf{a}_2 = \frac{a}{2}(3, -\sqrt{3}) \quad (2.1)$$

The corresponding reciprocal lattice is given by,

$$\mathbf{b}_1 = \frac{2\pi}{3a}(1, \sqrt{3}), \mathbf{b}_2 = \frac{2\pi}{3a}(1, -\sqrt{3}) \quad (2.2)$$

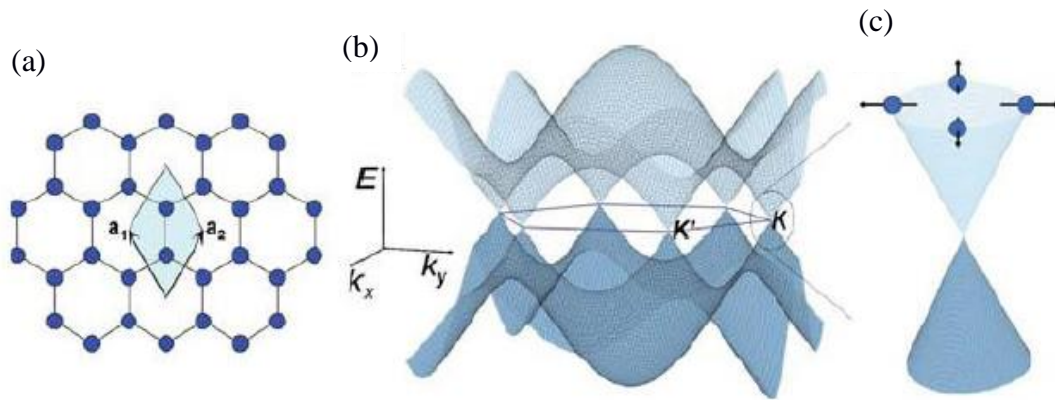


Fig. 2.5: Band structure of graphene: (a) Graphene honeycomb lattice. (b) tight-binding band structure of graphene [59] (c) Band structure close to the Dirac Point.

This linear relation also indicates that the electrons in it are mass-less. As we know, in solid state physics, the electron properties of materials are dominated by the Schrödinger equation, with an effective mass correspondence to the curvature of the band structure of the material. But this wouldn't apply to graphene, whose band structure is linear with no curvature. In graphene, its charges mimic relativistic particles and are dominated by Dirac Equation rather than Schrödinger Equation, and are therefore called Dirac Fermions. To study and describe the properties, quantum electrodynamics (QED) must be applied. The mass less Dirac fermions in graphene behave as though the speed of light is just 10^6 m/s, rather than 3×10^8 m/s, so graphene could allow us to investigate the fundamental interactions of matter without the need for huge particle accelerators.

2.6 Two Dimensional (2D) SiC₂

The optimized g-SiC₂ siligraphene crystallizes in the hexagonal space group, $P\bar{6}2m$ (no. 189), with $a = 5.019$ Å (Figure 1a and b) [60]. As similar as in the pure carbon graphene, Si adopts an undistorted trigonal coordination with a Si-C distance of 1.798 Å and bond angle of 120° . The C1 atom at the Wyckoff $1b$ site is also trigonally coordinated without any distortion. The C2 atom at the $3g$ site is in a distorted trigonal coordination with bond angles of 126.3 and 107.4° and bond distances of 1.798 and 1.445 Å. Such a small distortion comes from the radius and electronegativity differences between Si and C atoms, which also results in the electron polarization along the Si-C bond.

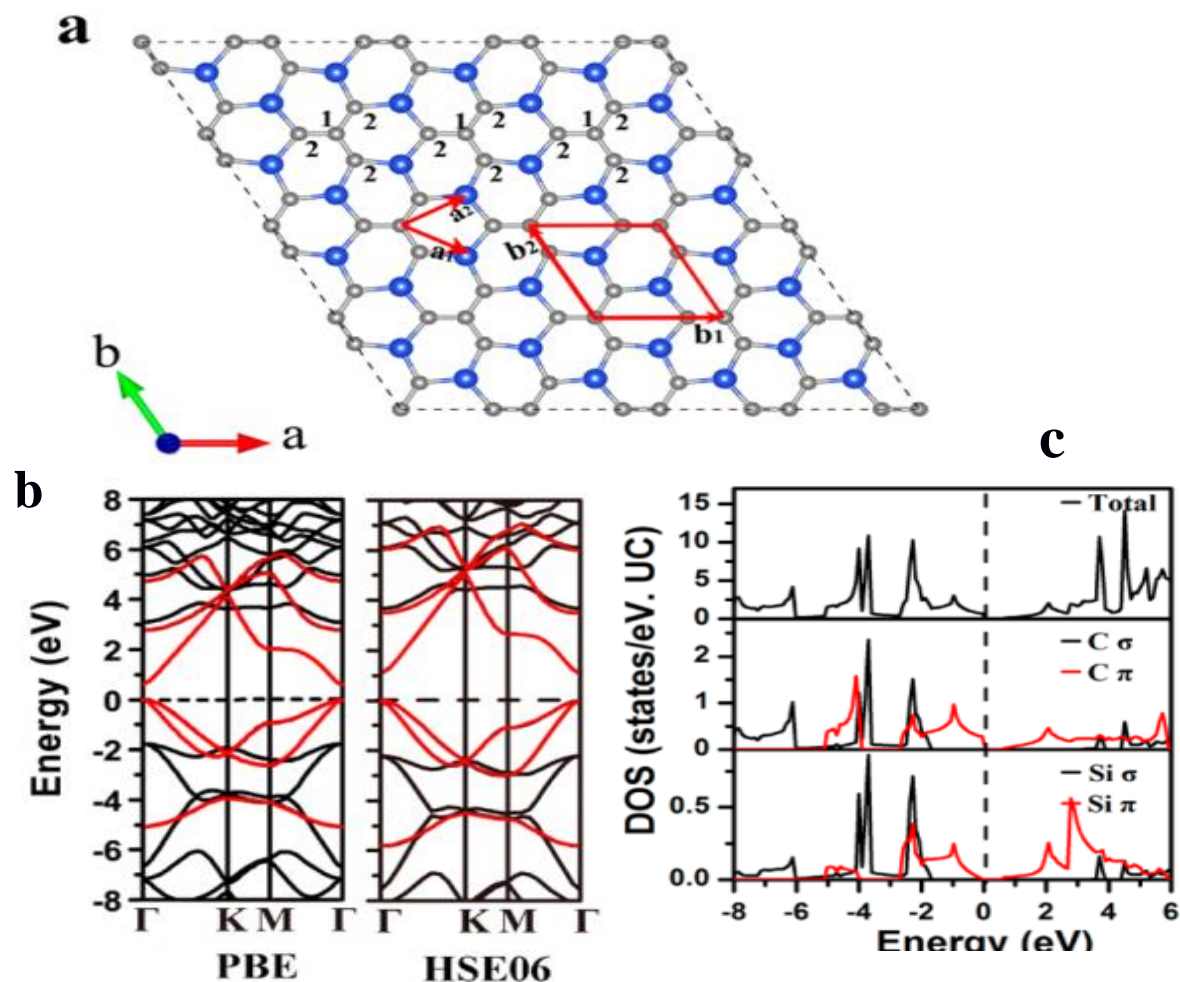


Fig. 2.6 (a) Optimized structure of g-SiC₂ siligraphene with unit cell outlined as red lines. Red vectors: a_1 , a_2 : graphene lattice vectors, (b) the band structure of g-SiC₂ monolayer calculated based on PBE and HSE06. The π bands are marked in red. (c) The total DOS and projected DOS (PDOS) of g-SiC₂ siligraphene. The Fermi energy is set as zero [60].

Nevertheless, this distortion is limited within the g-SiC₂ plane and does not push the C₂ atom out of the plane. As a resemblance of the pure carbon graphene, the gSiC₂ siligraphene features sp²-hybridization of C and Si atoms. The C-C bond (1.445 Å) shows the characteristic of a weak C=C double bond because it is slightly longer than the double C=C bond (for example, 1.332 Å in pt-SiC₂, [61] 1.33 Å in ethylene) and that in graphene (1.42 Å), but shorter than the 1.54 Å single C-C bond in ethane [62].

2.7 Two Dimensional (2D) SiC₇

The stability of g-SiC₇ siligraphene has been confirmed in the previous work [named (2, 0) structure according to its super lattice vector]. Here we performed more detailed calculations to verify it. First, the binding energy of g-SiC₇ siligraphene is calculated as 7.07 eV per atom, lower than that of graphene (8.66 eV per atom) but higher than the reported g-SiC₂ siligraphene (6.46 eV per atom) and g-SiC₃ siligraphene (6.70 eV per atom) [63]. This is mainly due to the fact that the Si atom tends to adopt a sp^2 - sp^3 hybridization to form the buckled pattern as silicene, which is greatly different from the pure sp^2 hybridization in graphene, leading to the phenomenon that the more Si atoms in planar siligraphene, the lower the stability [64]. The band structure displayed in Fig. 2.7a indicates that both the valence band maximum (VBM) and conduction band minimum (CBM) locate at the K point, showing a preferable efficiency of light absorption [65].

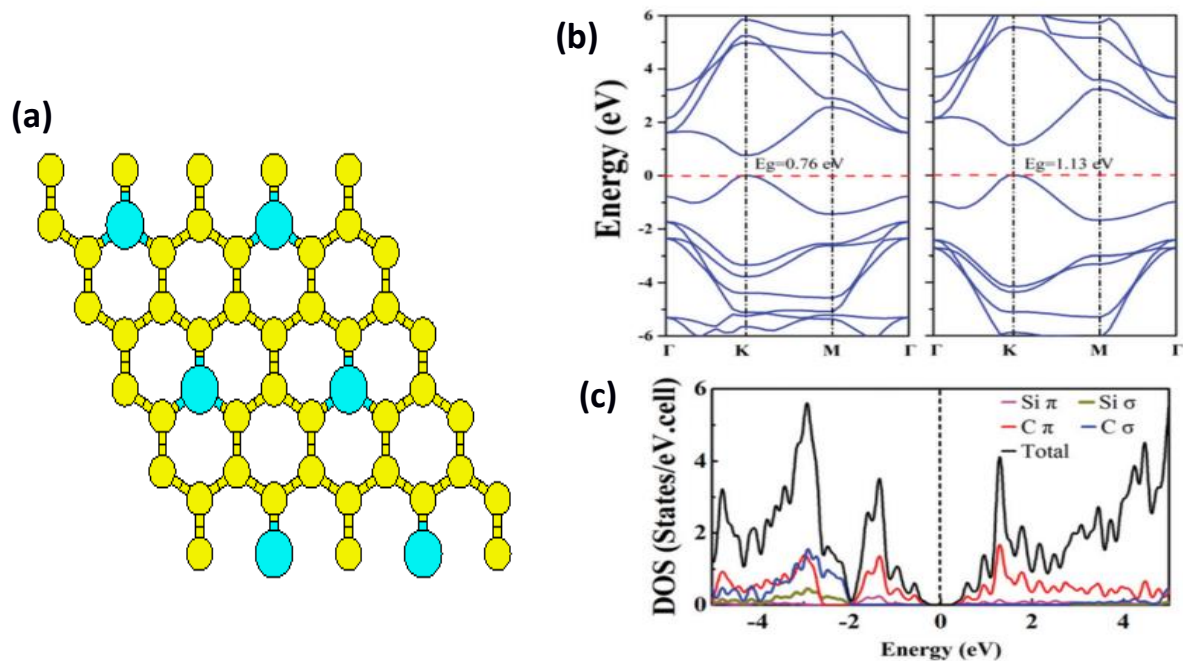


Fig. 2.7: (a) The optimized structure of g-SiC₇ siligraphene. (b) Band structure of g-SiC₇ siligraphene based on GGA-PBE (left panel) & HSE06 (right panel) calculations, respectively. Fermi level is set as zero and (c) Projected density of states (PDOS) of g-SiC₇ siligraphene. [66].

2.12 Two Dimensional (2D) SiC

Among the different two dimensional materials, SiC which is binary compound of carbon and silicon exhibits unique electronic and optical properties and thus has been a key material for high power and high temperature device applications. Also, several points are worth noting: C and Si-based 2D nanomaterials are extremely rare, and few examples are known, that is, graphene, SiC sheet, silicene, and pt-SiC₂; SiC₇ [66] and most of them are either metal or semimetal; (iii) band gaps of their derivative nanotubes are usually dependent on the chirality or/and the tube diameter. Theoretical calculations have also proposed that 2D-SiC with a honeycomb structure, similar to graphene and silicene, could be energetically stable. 2D honeycomb SiC unit cell can be thought of a graphene like unit cell with one carbon atom replaced by a silicon atom. As Si has a larger radius than C, the lattice gets extended.

The dynamically favorable planar structure is found buckling free with Si-C bond length of 1.75 Å, larger than the corresponding C-C bonds in graphene (1.42 Å). The Si-C-Si and C-Si-C bond angles are 120°. The 2D-SiC is produced by the sp² orbital hybridization combining σ-bonds and π-bonds.

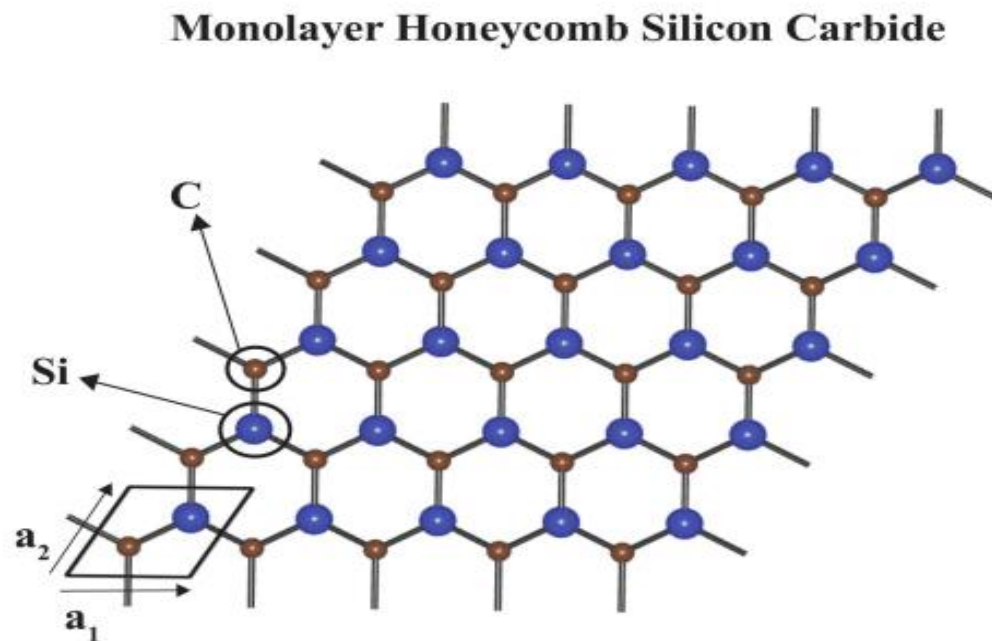


Fig. 2.9: Unit cell and lattice vectors of planar honeycomb SiC.

The σ -bond is formed by the silicon (Si-2s, 3p_x, 3p_y) and carbon (C-1s, 2p_x, 2p_y) electrons and the π -bond is generated by the Si-3p_z and C-2p_z electrons. The conduction and valence band edges at the K point are constructed by the π and π^* -bands, which is formed due to the bonding and anti-bonding combination of Si-3p_z and C-2p_z orbitals.

Chapter

III

Theoretical Background

Chapter at a Glance

- | | |
|--|--------------|
| • Introduction | Section 3.1 |
| • Schrödinger equation and its Hamiltonian | Section 3.2 |
| • Born-Oppenheimer approximation | Section 3.3 |
| • The Hartree approximation | Section 3.4 |
| • The Hartree-Fock approximation | Section 3.5 |
| • The correlation energy | Section 3.6 |
| • The Hohenberg-Kohn theorems | Section 3.7 |
| • The exchange-correlation approximations | Section 3.8 |
| • The Kohn-Sham theorem | Section 3.9 |
| • Pseudopotential | Section 3.10 |
| • Spin-Orbit coupling effect | Section 3.11 |
| • Phonon properties | Section 3.12 |
| • Thermal properties | Section 3.13 |
| • Quantum Espresso | Section 3.14 |
| • Computational details | Section 3.15 |

3.1 Introduction

For many theories in condensed matter physics, the modeling is typically empirical or semi-empirical based on some experimentally measured macroscopic phenomena. It is often possible to predict the unknown behaviors of systems by interpolating or extrapolating these models. In contrast, the first principles method starts from our fundamental understanding of the condensed matter systems. For instance, crystals are made of positively charged nuclei and electrons held together by the coulomb interaction. Without any approximation, the behavior of any system can be fully described if we can precisely solve this model. Unfortunately, the difficulty in this model is not the theory but the size effect of systems from the perspective of computational resources. Various theories have been proposed to make this model solvable.

In this chapter, it will briefly introduce one of them, namely density functional theory, which is also used in our work to investigate the structural, electronic and vibrational properties in 2D-SiC. In the first section, we start from the Schrödinger equation and Born-Oppenheimer approximation, which separates the description of nuclei and electrons so as to largely simplify the solution. Next, the Hohenberg-Kohn theorem will be introduced, which proves a one-to-one correspondence of the system's ground state electron density to the external potential. Based on the Hohenberg-Kohn theorem, Kohn-Sham equation, the main equation in density functional theory, is derived. Meanwhile, the nature of two well-known exchange-correlations functional is covered briefly. It will also discuss three bases used to solve the Kohn-Sham equations and the convergence test in first principles calculation. Finally, it will deliberate about computational method for calculating different properties.

3.2 Schrödinger equation and its Hamiltonian

All materials are composed of atomic nuclei and electrons. The macroscopic material properties that we observe only depend on the position of these electrons and ions. Thus, knowing only the type of atoms the material is made of is in principle enough to calculate the wave function and energy of the system using the (time independent) Schrödinger equation-

$$H\Psi(r_1, r_2, \dots, R_1, R_2, \dots) = E\Psi(r_1, r_2, \dots, R_1, R_2, \dots) \quad (3.1)$$

Where Ψ is the wave function of the system, \mathbf{r}_i and \mathbf{R}_i are the positions of the electrons and ions, respectively, and H is the Hamiltonian of the system:

$$H = -\sum_i \frac{\hbar^2 \nabla_i^2}{2m_e} - \sum_{i,I} \frac{1}{4\pi\epsilon_0} \frac{Z_I e^2}{|r_i - R_I|} + \frac{1}{2} \sum_{i \neq j} \frac{1}{4\pi\epsilon_0} \frac{e^2}{|r_i - r_j|} - \sum_I \frac{\hbar^2 \nabla_I^2}{2M_I} + \frac{1}{2} \sum_{I \neq J} \frac{1}{4\pi\epsilon_0} \frac{Z_I Z_J e^2}{|R_I - R_J|} \quad (3.2)$$

Here, M_I and Z_I are the nucleus mass and charge respectively, and m_e is the electron mass. This Hamiltonian can be decomposed in five terms-

$$H = T_e + V_{ext} + V_{int} + T_N + V_N \quad (3.3)$$

Where T_e and T_N is the kinetic energy operator of electrons and nuclei, respectively, V_{ext} is the potential energy of the electrons in a field of nuclei, V_{int} represents the Coulomb interaction between the electrons and similarly V_N is the Coulomb interaction between nuclei. These calculations are known as first-principles or ab-initio calculations since they are based only on the laws of physics and the values of nature's constants, such as Planck's constant \hbar and the electron charge e . Nothing else is assumed or used as empirical input. In practice, however, it is only possible to solve the Schrödinger equation exactly for small, simple systems such as the hydrogen atom with spherical symmetry. For larger systems like molecules and solids, additional approximations have to be made. Note that hereafter we will make use of atomic units to simplify the formulas. In atomic units we have $\hbar = m_e = e = 4\pi\epsilon_0 = 1$.

3.3 Born-Oppenheimer approximation

The Born-Oppenheimer approximation separates the motion of the ions and the electrons. This is justified by the fact that the mass of a nucleus is much larger than the mass of an electron so that they move on different time scales. From the electron point of view, the ions are stationary and the electron cloud will rearrange itself instantaneously to any new ionic configuration.

Mathematically, the wave function is rewritten as a product of the electron wave function and the nuclear wave function-

$$\Psi(r_1, r_2, \dots, R_1, R_2, \dots) = \Psi(r_1, r_2, \dots, R_1, R_2, \dots) \cdot \chi_{nuc}(R_1, R_2, \dots) \quad (3.4)$$

The semicolon in the electron wave function indicates that it is dependent upon the ionic

positions as parameters but not as variables. The Schrödinger equation of the electrons for a given frozen ionic configuration is written as follows:

$$H'\Psi(r_1, r_2, \dots, R_1, R_2, \dots) = E'\Psi(r_1, r_2, \dots, R_1, R_2, \dots) \quad (3.5)$$

H' represents the electronic Hamiltonian consisting of only electronic terms:

$$H = T_e + V_{ext} + V_{int} \quad (3.6)$$

And the total Hamiltonian is then reduced to:

$$H = T_e + V_{ext} + V_{int} + V_N \quad (3.7)$$

With the Born-Oppenheimer approximation, the original problem is now reformulated as a quantum many-body problem for the electrons in a Hamiltonian set by the nuclei positions. The last, and probably hardest, obstacle to overcome is the reduction of the many-electron equation above to a solvable problem.

3.4 The Hartree approximation

The simplest way to solve the many-electron equation is to rewrite Eq.(3.5) as a one-particle equation for an electron moving in an average potential from all the electrons, as proposed by Hartree. The wave function, then becomes-

$$\Psi(r_1, r_2, \dots, r_n) = \varphi_1(r_1), \varphi_2(r_2) \dots \dots \varphi_n(r_n) \quad (3.8)$$

The $\varphi_i(\mathbf{r}_i)$ is n independent electron wave functions. A fundamental result in quantum mechanics states that if E_0 is the ground state energy solution of the Schrödinger equation, for any wave function-

$$\frac{\langle \varphi | H | \varphi \rangle}{\langle \varphi | \varphi \rangle} \geq E_0 \quad (3.9)$$

This is called the vibrational principle. This principle can be used with the Hamiltonian in Eq.(3.3) and the constraint that the wave function should have the Hartree form (presented in Eq.(3.8)) to prove that the solution to the Schrödinger equation in the Hartree approximation is obtained by solving the Hartree equation-

The effect of the new constraint is to add a term, called the exchange potential, to the Hartree Eq.(3.10).

3.6 The correlation energy

The Hartree-Fock approach, assuming independent electrons in an effective potential is an approximation to the true many-body problem. The energy missing is defined as the correlation energy ($E_{corr} = E_{exact} - E_{HF}$). Many methods exist to introduce this correlation energy very accurately for instance Møller-Plesset (MP) perturbation theory, configuration interaction (CI), or coupled cluster (CC) methods or quantum Monte-Carlo methods [67]. However, these methods are computationally very expensive and only the smallest systems can be currently computed. On the other hand, Density Functional Theory (DFT) offers a good compromise between the qualitative description of electronic structure and the computational effort required to produce the result. Thus DFT is one of the most popular and successful quantum mechanical approaches to describe matter. It is nowadays routinely applied for calculating, e.g., the binding energy of molecules in chemistry and the electronic band structure of solids in physics. In this thesis, we apply DFT to solve the electronic Hamiltonian for periodic crystals.

3.7 The Hohenberg-Kohn theorems

Modern theory of DFT is based on the two Hohenberg-Kohn (HK) theorems [69]: the first theorem states that the many-body wave function, which has a central position in standard quantum theory, can be replaced by the electronic ground state density without any loss of information and the second theorem is more or less the equivalent of the variational principle in standard quantum mechanics. In DFT the electron density is the central quantity. In a system of n electrons the electron density is defined from the wave functions as follows,

$$n(r) = \sum_{i=1}^N \int \cdots \int dr_1 \cdots dr_n \Psi^*(r_1, \cdots, r_N) \delta(r_i - r) \Psi(r_1, \cdots, r_N) \quad (3.14)$$

The energy is now rewritten from being the expectation value of the electronic Hamiltonian to a functional only depending on the electron density and not explicitly the wave function. The first Hohenberg-Kohn theorem is:

Theorem 1. *For any system of interacting particles in an external potential $V_{ext}(\mathbf{r})$ the potential $V_{ext}(\mathbf{r})$ is determined uniquely, except for a constant, by the ground state density $n_0(\mathbf{r})$.*

This implies that all the properties can thus be extracted from the exact ground state electron density. The problem is now only how to find this density. The second theorem based on the variational principle is helpful in this matter.

Theorem 2. *A universal function for the energy $E[n]$ in terms of the density $n(\mathbf{r})$ can be defined, valid for any external potential $V_{ext}(\mathbf{r})$. The exact ground state energy of the system is the global minimum of this function and the density that minimizes the functional is the exact ground state density $n_0(\mathbf{r})$.*

This reduces the very complex problem of finding all ground state physical properties of a system to finding the minimum of the energy with respect to the electron density. The energy function is as follows:

$$E_{HK} = T[n] + E_{int}[n] + \int V_{ext}(r)n(r)dr \quad (3.15)$$

Where $E_{HK}[n]$ is the total energy functional, $T[n]$ its kinetic energy part and $E_{int}[n]$ the part coming from the electronic interactions. E_N does not depend on the density and is due to the nuclei-nuclei interaction. It should be noted that although the first Hohenberg-Kohn theorem, require a non-degenerate ground state, degenerate ground states are also allowed by the Levy formulation [68]. It should also be noted that using the Hohenberg Kohn formulation of DFT implies that we are working at $T = 0$ K.

3.8 The exchange-correlation approximations

3.8.1 The local density approximation:

The simplest physical way to approximate the exchange-correlation energy is the Local Density Approximation (LDA). In this approximation two assumptions are made: i) the local exchange-correlation energy per particle only depends on the local density (hence the name of the approximation) and ii) is equal to the exchange-correlation energy per particle of a homogeneous electron gas, which has the same density, in a neutralizing positive background. The total exchange-correlation energy E_{XC} is then given by the sum of the contributions of each point in

space, where it is assumed that the contribution of one point only depends on the density of that particular point, independent of the other points. So-

$$E_{XC}[n] = \int n(r) \epsilon_{XC}(n(r)) dr \quad 3.16$$

Where $\epsilon_{XC}(n(r))$ is the exchange-correlation energy per particle of a uniform electron gas of density $n(\mathbf{r})$. The quantity $\epsilon_{XC}(n(r))$ can be further split into exchange and correlation contributions,

$$\epsilon_{XC}(n(r)) = \epsilon_X(n(r)) + \epsilon_C(n(r)) \quad 3.17$$

The exchange parts, X , represent the exchange energy of an electron in a uniform electron gas and are given by-

$$\epsilon_X = \frac{-3}{4} \sqrt[3]{\left(\frac{3n(r)}{\pi}\right)} \quad 3.18$$

The correlation part, C , is determined using quantum Monte-Carlo simulations of the homogeneous electron gas as proposed by Ceperly and Alder [70]. This approximation is more accurate for systems with slowly varying densities, as it is assumed that the density is locally a constant. While being a simple approximation, the results of this approximation are surprisingly good. In general, LDA almost always leads to a correct picture of binding trends across the periodic table.

3.8.2 The generalized gradient approximation

In LDA one uses the knowledge of the density at a point \mathbf{r} . In real systems the density varies in space. A logical improvement of the LDA approximation would be to include also information of this rate of change in the function. This can be done by adding gradient terms. This approach is called the gradient-expansion approximation. In this class of approximation one tries to systematically calculate gradient-corrections of the form $|\nabla n(r)|$, $|\nabla n(r)|^2$, $|\nabla^2 n(r)|$, etc., to the LDA. In practice, the inclusion of low-order gradient corrections almost never improves on the LDA, and often even worsens it. Moreover, higher-order corrections are exceedingly difficult to calculate and little is known about them. It was realized that instead of power-series like

systematic gradient expansions, one could experiment with more general functions of $n(\mathbf{r})$ and $|\nabla n(\mathbf{r})|$, which need not proceed order by order. Such functional, of the general form-

$$E_{XC}[n]^{GGA} = \int \epsilon_{XC}(n, |\nabla n|, \nabla^2 n) dr \quad 3.19$$

It is known as generalized-gradient approximations (GGAs). The current GGAs seem to give reliable results for all main types of chemical bonds and are popular in computational chemistry. We have used the Perdew-Burke Ernzerhof (PBE) version of GGA [71] in this work.

3.9 The Kohn-Sham theorem

The Hohenberg-Kohn theorems show that the electron density can be rigorously made the fundamental quantity of the many-body problem, but they are pure theorems of existence and say nothing about how this exact charge density can be found. Kohn and Sham have shown that there is a way to map the problem of solving Eq. (3.15) to the one of solving a system of non-interacting electrons moving in an effective potential from all the (other) electrons. According to Theorem 2, the true electron density will minimize the total energy, but all means of finding it are valid. It could be guessed or, as suggested by Kohn and Sham [72], calculated from a reference system of non-interacting electrons moving in an effective potential. Thus, developing this variation with the full energy functional added (Eq. (3.15)), under the condition that the sum of the density throughout the molecule or solid should be constant and equal to the number of electrons, since the electron density,

$$\int_V n(\mathbf{r}) d\mathbf{r} = n_e \quad (3.20)$$

Finally gives the Schrodinger-like equations called the Kohn-Sham equations:

$$H\varphi_i = \left[-\frac{1}{2}\nabla^2 + V_{eff}(\mathbf{r})\right]\varphi_i = \epsilon_i \varphi_i \quad (3.21)$$

H is the one electron Hamiltonian and $V_{eff}(\mathbf{r})$ the effective potential in which the electron moves. The effective potential is given by-

$$V_{eff}(\mathbf{r}) = V_{ext} + V_H + V_{XC} = V_{ext}(\mathbf{r}) + \int \frac{n(\mathbf{r}')}{|\mathbf{r}-\mathbf{r}'|} d\mathbf{r}' + \frac{\delta E_{XC}[n(\mathbf{r})]}{\delta[n(\mathbf{r})]} \quad (3.22)$$

Since the electron density,

$$n(\mathbf{r}) = \sum_{i=1}^{occ} |\varphi_i(\mathbf{r})|^2 \quad (3.23)$$

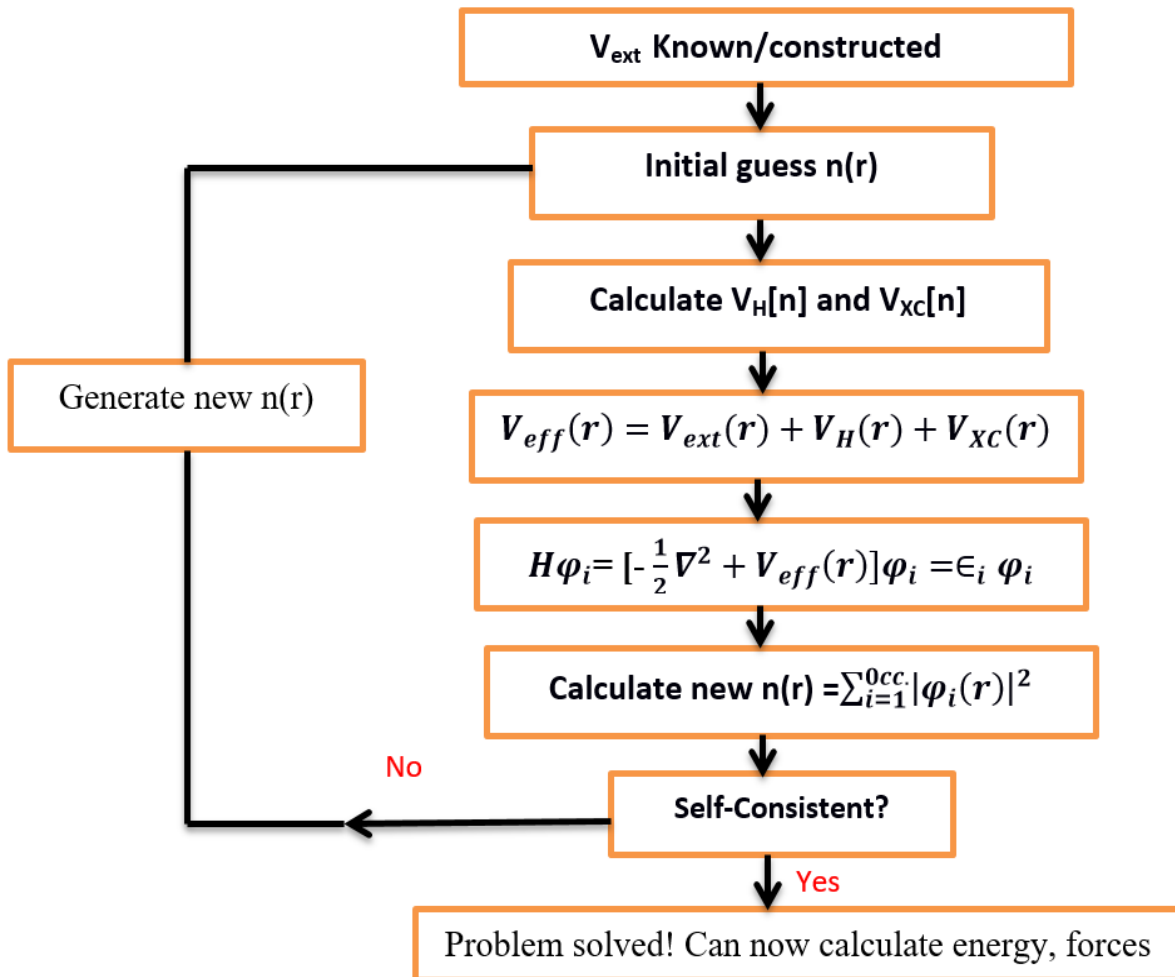


Fig. 3.1: Flowchart of Kohn-Sham Theorem.

It is needed to calculate the last two terms, which are the Coulomb potential from all electrons and the exchange-correlation potential; the Kohn-Sham equations need to be solved self-consistently. The new term, the exchange correlation potential, appearing here contains all the many-body effects that are not present in the classical Hartree interaction term. The initial electron density can be chosen, for example, as a superposition of atomic densities. The Kohn-Sham equations can now be solved instead of finding the minimum of Eq. (3.15), and the orbitals $\varphi_i(\mathbf{r})$ then give the electron density according to Eq. (3.19) above. These orbitals are often called Kohn-Sham orbitals and in the case of a non-spin-polarized system, each of these orbitals contains two electrons. (To deal with the spin-related effects, the total density is instead expressed as the sum of the spin-up and spin-down densities $n(\mathbf{r}) = n\uparrow(\mathbf{r}) + n\downarrow(\mathbf{r})$).

In the fig. 3.1 shows the flowchart and we consider the charge density as the quantity to be determined self consistently. We supply an input charge density to the Kohn-Sham equations and we get an output charge density. At self-consistency the first algorithm come to mind is simply use the output charge density as the new input charge density. The new input charge density is generated by mixing the input and output charges. If the new wave function (charge density) or the energy is consistent with the old one, we reach at the point of self-consistency. After the problem is solved the solved equation can be used to calculate the energy, forces, bulk modules, etc.

3.10 Pseudopotential

When people numerically calculate the electronic structure in materials, a highly efficient and easily implemented algorithm is needed. The plane wave method is one of the most hopeful candidates, and the orthogonal plane wave method (OPW) is widely used in the early calculations [73]. However, the deep and sharp nuclei attractive potential makes the number of plane waves in OPW very large and slows the calculation speed extremely. To avoid this difficulty, people suggest many models, and the pseudo-potential is one of the successful solutions. The key point of the pseudo-potential is that the core electron states are not changed much under different chemical environments. The main contribution of the core electron states is to make the valence electron orthogonal to them. So we can model the effect as a potential, which is repulsive because of the orthogonally. This repulsive potential can cancel part of the sharp and deep nuclei ionic potential and decreases the number of plane waves needed to expand the electronic states in solids. The pseudo-potential was first introduced by Fermi in 1934, and was popular after the 1950's. We start this section from the Philips-Kleinman cancellation theorem under the OPW method [38].The general form of valence electron states can be written with-

$$\langle \Psi \rangle = \langle \Phi \rangle + \sum C_{core} \langle \Phi_{core} \rangle \quad (3.24)$$

Where the part $\langle \Phi_{core} \rangle$ is the core electron state and has the sharp oscillation. $\langle \Phi \rangle$ is hoped to be the smooth part of the electron states. Since the valence electron states are orthogonal to the core states, we have-

$$C_{core} = -\langle \Phi_{core} | \Phi \rangle \quad (3.25)$$

Then substitute Eq. (2.18) into the static Schrodinger equation $H\langle\Psi\rangle = E\langle\Psi\rangle$, we get-

$$H\langle\Phi\rangle - \sum E_{core}\langle\Phi_{core}|\Phi\rangle\langle\Phi_{core}\rangle = E\langle\Phi\rangle - \sum\langle\Phi_{core}|\Phi\rangle\langle\Phi_{core}\rangle \quad (3.26)$$

We can rearrange the formula to

$$H + \sum_{core}(E - E_{core})\langle\Phi_{core}|\Phi\rangle\langle\Phi_{core}\rangle = E\langle\Phi\rangle \quad (3.27)$$

The new operator $\sum_{core}(E - E_{core})\langle\Phi_{core}|\Phi\rangle\langle\Phi_{core}\rangle$ shown with the original Hamiltonian acts like a potential term, and is defined as the pseudopotential

$$V_{ps} = \sum_{core}(E - E_{core})\langle\Phi_{core}|\Phi\rangle\langle\Phi_{core}\rangle \quad (3.28)$$

With the help of the pseudopotential, the Schrodinger equation can be rewritten as

$$H + V_{ps}\langle\Phi\rangle = E\langle\Phi\rangle \quad (3.29)$$

Because $\langle\Phi\rangle$ is the smooth part of the wave function $\langle\Psi\rangle$, the solution to Eq. (3.23) needs a much smaller number of plane waves and improves the efficiency of the calculation significantly. So the plane wave method in conjunction with the pseudopotential is very popular in numerical calculations. In the point view of physics, the pseudopotential term V_{ps} acts as a repulsive potential, because the energy of valence electrons is always higher than that of core electrons. It is also short-ranged because the core electronic state is close to the nuclei.

As a result, the repulsive and short-range pseudopotential cancels the sharp and deep part of the ionic nuclei potential. Furthermore, as shown in Eq. (3.21), the pseudopotential method gives the same eigenvalue despite of the wave function is replaced with the pseudo wave function, which is favorable in numerical calculations. There are mainly two types of pseudopotentials. One is the empirical pseudopotential, and the other one is called ab initio pseudopotential. The first one uses the parameterized pseudopotential to fit known experimental results and to calculate new properties of materials with this fitted pseudopotential. But this method needs those parameters, which are strongly depending on the fitting process and cannot be thought as a complete first-principles approach. Alternately, one can directly calculate core electron states with density functional theory and construct the pseudopotential without fitting to experiment, which is called the ab initio pseudopotential. This ab initio pseudopotential has really good transferability and accuracy. It is widely used in today's first-principles calculations.

3.11 Spin-Orbit coupling effect

Spin-orbit coupling (SOC) is an essential ingredient for quantitatively correct energy band structures of materials composed of any but the few lightest elements, appearing in materials applications as diverse as heavy-light hole masses in conventional semiconductors. Spin-orbit coupling (SOC) is the interaction between the spin of the electron and its angular motion. The effect of SOC causes a lift in the degeneracy of the one-electron energy levels due to the electromagnetic interaction between the spin and the magnetic field generated by the orbital motion of the electron. The simplest form of Schrodinger equation in solid state physics neglects the spin-dependent term in the Hamiltonian, so the energies obtained are doubly degenerate spin-up and spin-down states. However, we can include a SOC term by considering the relativistic correction to the Schrödinger equation. To incorporate the SOC effect on the band structure, the effective spin orbit coupled Hamiltonian was included in the Kohn-Sham DFT calculations. The total Hamiltonian for Kohn-Sham DFT calculations, including the SOC Hamiltonian can be formed as-

$$\begin{aligned}\hat{H} &= \frac{\hat{p}^2}{2m_a} + \hat{V}_{ext}(\hat{r}) + \hat{V}_{es}(\hat{r}) + \hat{V}_{xc}(\hat{r}) + \hat{H}^{SOC} \\ &= \frac{\hat{p}^2}{2m_a} + \hat{V}_a(\hat{r}) + \hat{H}^{SOC}\end{aligned}\quad (3.30)$$

Where, \hat{V}_{ext} is the external potential, \hat{V}_{es} is the electrostatic or Hartree potential, \hat{V}_{xc} is the exchange-correlation potential, \hat{H}^{SOC} is the spin-orbit coupling operator, and \hat{V}_a is the applied field or Kohn-Sham potential. The Hamiltonian equation for SOC can be derived from a nonrelativistic approximation to the Dirac equation [74] by considering the relativistic limit as follows-

$$\hat{H}^{SOC} = \frac{\hbar}{4m_a^2c^2} (\nabla \hat{V}_a \times \hat{p}) \cdot \hat{s} \quad (3.31)$$

Here, \hat{p} is the momentum and \hat{s} denotes the spin operators of electrons. Considering central field approximation, \hat{H}^{SOC} becomes-

$$\hat{H}^{SOC} = \xi(\hat{r}) \hat{l} \cdot \hat{s} \quad (3.32)$$

Where \hat{S} is the total electronic spin operator, \hat{l} is the total atomic angular momentum and $\xi(\hat{r}) = \frac{1}{2m_a^2 c^2 r} \frac{dV_a}{dr}$.

3.12 Phonon properties

Phonons determine the crystal temperature. Knowledge of phonon characteristics are required to describe mechanical, acoustic, dynamical, spectroscopic and thermodynamic properties of crystals at finite temperature. The easiest and perhaps the most effective approach to calculate phonon frequencies and eigenvectors from first-principles are to use existing and well-tested software's bases on the density functional software (DFT). Usually, at $T = 0$ the ground state energy E as a function of atomic positions $\mathbf{R}(\mathbf{n}, \mu)$, where \mathbf{n} is the primitive unit cell index and μ is the atomic index, is expanded over small displacements $\mathbf{U}(\mathbf{n}, \mu)$ up to harmonic term [75]. Any atomic displacement $\mathbf{U}(\mathbf{m}, \nu)$ generates HF forces on all other atoms of the determined supercell according to the relationship-

$$F_i(\mathbf{n}, \mu) = - \sum_{\mathbf{m}, \nu, j} \Phi_{i,j}(\mathbf{n}, \mu, \mathbf{m}, \nu) U_j(\mathbf{m}, \nu) \quad (3.33)$$

This relates the generated forces with the force constant matrices and atomic displacement. Knowing the displacements and arising HF forces one is able to determine the force constants $\Phi_{i,j}(\mathbf{n}, \mu, \mathbf{m}, \nu)$. The dynamical matrix is defined as-

$$D(k; \mu, \nu) = \frac{1}{\sqrt{M_\mu M_\nu}} \sum_{\mathbf{m}} \Phi(0, \mu; \mathbf{m}, \nu) \exp\{-2\pi i \mathbf{k} \cdot [\mathbf{R}(0, \mu) - \mathbf{R}(\mathbf{m}, \nu)]\} \quad (3.34)$$

Here, summation \mathbf{m} runs over all primitive unit cells of the crystal, M_μ, M_ν are masses of atoms, and \mathbf{k} is the wave vector. Diagonalization of the dynamical matrix-

$$\omega^2(k, j) \mathbf{e}(\mathbf{k}, j) = D(\mathbf{k}) \mathbf{e}(\mathbf{k}, j) \quad (3.35)$$

Here, gives the phonon frequencies $\omega^2(k, j)$ and eigenvectors $\mathbf{e}(\mathbf{k}, j)$, called also polarization vectors.

3.13 Thermal properties

Once phonon frequencies over the Brillouin zone are known, from the canonical distribution in statistical mechanics for phonons under the harmonic approximation, the energy of phonon system can be obtained [76]. The thermal properties of solids at constant volume can be calculated from their phonon density of states as a function of frequencies. The phonon contribution to the Helmholtz free energy F_A is given by:

$$F_A = \frac{1}{2} \sum_{q,v} \hbar \omega_{q,v} + k_B T \sum_{q,v} \ln[1 - \exp(-\hbar \omega_{q,v}/k_B T)] \quad (3.36)$$

Where k_B and \hbar are the Boltzmann constant and the reduced Planck constant, respectively, \mathbf{q} and ν are the wave vector and band index, respectively, $\omega_{\mathbf{q},\nu}$ is the phonon frequency at \mathbf{q} and ν , and T is the temperature.

3.14 Quantum Espresso

Quantum ESPRESSO is a software suite for ab initio quantum chemistry methods of electronic-structure calculation and materials modeling, distributed for free under the GNU General Public License. It is based on Density Functional Theory, plane wave basis and pseudo-potentials (both norm-conserving and ultra-soft). ESPRESSO is an acronym for opEn-Source Package for Research in Electronic Structure, Simulation, and Optimization [77]. The core plane wave DFT functions of QE are provided by the PWscf component, PWscf previously existed as an independent project. PWscf (Plane-Wave Self-Consistent Field) is a set of programs for electronic structure calculations within density functional theory and density functional perturbation theory, using plane wave basis sets and pseudo-potentials. The software is released under the GNU General Public License. It is a merge of several pre-existing packages and provides access to several techniques whose usefulness has traditionally been hindered by the lack of available software: notably-

- Linear response
- Ultra soft PP
- Car-Parrinello Molecular Dynamics

There are two main packages in Quantum-ESPRESSO

1. CP/FPMD package

2. PWscf package

1. CP/FPMD package

Car-Parrinello variable-cell molecular dynamics with Ultrasoft PP's-

- “Grid Box” for fast treatment of augmentation terms in Ultrasoft PP's
- Various electronic and ionic minimization schemes: damped dynamics, conjugate gradient,

- Verlet dynamics with mass preconditioning
- Constrained dynamics
- Temperature control: Nos thermostat for both electrons and ions, velocity rescaling

2. PWscf package

- Self-consistent ground-state energy and Kohn-Sham orbitals, forces, structural optimization
- Spin-orbit and non-collinear magnetization
- Molecular dynamics on the ground-state Born-Oppenheimer surface (no Car-Parrinello Dynamics)
- Variable-cell molecular dynamics with modified kinetic functional
- Nudge Elastic Band (NEB) and Fourier Strings Method schemes for transition paths, energy barriers PWscf package, Linear Response
- Phonon frequencies and eigenvectors at a generic wave vector, interatomic force constants in real space, effective charges and dielectric tensors, electron-phonon interaction coefficients for metals
 - Third-order a harmonic phonon lifetime, non-resonant Raman cross sections
 - Macroscopic polarization, finite electric fields with Berry's phase Perspectives and future developments.
- Calculation of NMR chemical shifts
- Exact-exchange calculations
- Projector-Augmented Waves (PAW)
- Time-Dependent DFT (TD-DFT).

3.15 Computational details

The first-principle calculations were performed using the density functional theory as implemented in the Quantum espresso package. Ultra-soft pseudo potential with the Perdew-Wang exchange-correlation function within the local density approximation (LDA) was employed to calculate the structural relaxation and total energy of the system. The calculations were performed on a single layer 2D-SiC consisting of two atom basis primitive unit cell and in 2D-SiC (4×4 supercell) structure was consisting of 32 atoms. The kinetic energy cutoff and the charge density cutoff used were 30 Ry and 200 Ry, respectively. The convergence threshold was 10^{-6} Ry/atom. The irreducible Brillouin Zone was sampled with a Gamma-centered $12 \times 12 \times 1$ Monkhorst-Pack k- points for the band structure and density of state calculation. The electronic properties were also calculated using the quantum espresso package with considering the SOC. The kinetic energy cutoff, the charge density cutoff and Monkhorst-Pack k- points are similar with the excluding SOC. The electronic properties of single vacancy defect (silicon and carbon) of 2D-SiC (4×4 supercell) was also performed by the same method.

To ensure the dynamical stability of the lowest energy structure of 2D-SiC, phonon dispersion characteristics were also calculated using the density functional perturbation theory (DFPT) [76]. The norm conserving pseudopotential with local density approximation and the dynamical matrix $2 \times 2 \times 2$ has been used for phonon calculation. The splitting of longitudinal and transverse optical modes at Γ was taken into account via the method of Born and Huang [77]. The Raman peaks are extracted from the DFPT calculation of second order response to an electric field which is implemented in the Quantum espresso package.

In order to implement the QHA to calculate Helzmolt free energy from first principles, one needs to compute the complete phonon dispersion of a crystal for different values of the crystal volume. This can be done within DFT by the direct or frozen phonon method, or by the linear response method. The former does not require the use of specialized software beside that needed to perform standard ground-state DFT calculations, but is computationally more demanding. Some software tools that help analyze the output of standard DFT code to produce real-space IFC's and, from these, reciprocal-space dynamical matrices are available. As, for the linear response approach, have implemented on the general-purpose package Quantum espresso. In the

following we briefly describe the former, as well as other code, QHA, that can be used as a post-processing tool to perform QHA calculations starting from lattice-dynamical calculations performed with many different methods.

3.15 Different Steps for calculation-

3.15.1 Band Structure Calculation

- First to calculate self-consistent field (scf).
- Next to calculate non-self-consistent field (nscf).
- Then to calculate the band structure.

3.15.2 Electronic Density of states

- First to calculate self-consistent field (scf).
- Next to calculate non-self-consistent field (nscf).
- Then to calculate DOS.

3.15.3 Phonon Density of States calculation

- **Step 1. PW** Self consistent calculation of electron density. Outputs are wave functions.
- **Step 2. PH** Phonon calculation of linear response, with output on a rough grid.
- **Step 3.Q2R** Fourier transforms to real space and obtains force constants by interpolation.
- **Step 4. MATDYN** Then to calculate DOS using matdyn.x

The details of the calculation procedure for electronic and phonon properties using the first principle density functions, theory has been demonstrated by the block diagram as shown in below.

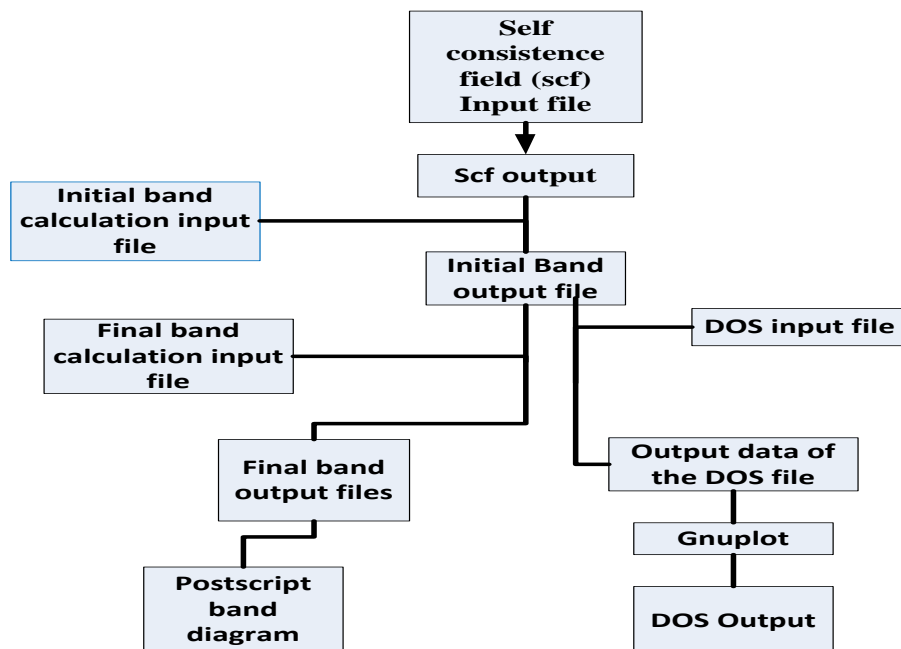


Fig. 3.2: Schematic for the calculation of electronic properties of novel 2D SiC.

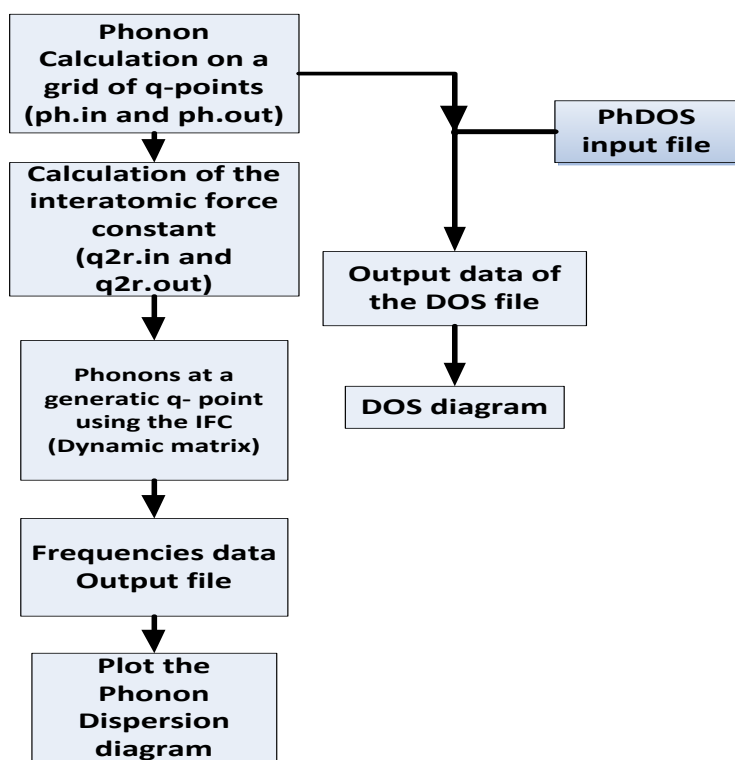


Fig. 3.3: Schematic for the calculation of phonon properties of novel 2D-SiC.

Chapter

IV

Results and Discussion

Chapter at a Glance

- | | |
|---|--------------------|
| • Structural properties | Section 4.1 |
| • Electronic properties without SOC effect | Section 4.2 |
| • Electronic properties with SOC effect | Section 4.3 |
| • Phonon properties | Section 4.4 |
| • Raman and infrared (IR) spectra | Section 4.5 |
| • Thermal properties | Section 4.6 |
| • Effect of vacancy defects on 2D-SiC | Section 4.7 |

4.1 Introduction

This chapter provides the important new findings of 2D-SiC including its structural, electronic and vibrational properties. It also provides that spin orbit coupling effect on electronic properties of both pure and defective structure of 2D-SiC.

4.2 Structural properties

Structural properties generally change due to the surface effects; we thus first optimize the atomic structure of the 2D-SiC. The initial configuration is generated placing one silicon atom and one carbon atom alternatively on the same plane, forming the 2-atoms-unit cell. The relaxed structure shows that the system is still coplanar as shown in Fig. 1(a). The dynamically favorable planar structure is found buckling free with Si-C bond length of 1.75 \AA , larger than the corresponding C-C bonds in graphene (1.42 \AA). The Si-C-Si and C-Si-C bond angles are 120° . The most stable lattice constant of planer 2D-SiC has been examined by calculating the total energy as a function of lattice parameter. Figure 2(a) portrays the variation of total energy as a function of the lattice constant. The total energy minimum of the relaxed structure is obtained at a lattice constant of 5.72 Ry , which is in very good agreement with the earlier computational and experimental works [44]. Besides lattice constant, the number of k-points mesh in Brillouin zone and kinetic energy cutoff affect the optimized structure and the accuracy of the calculations. The total energy with the variation of plane wave cut-off energy and k-points have also been carried out under PBE pseudo potential of the generalized gradient approximation.

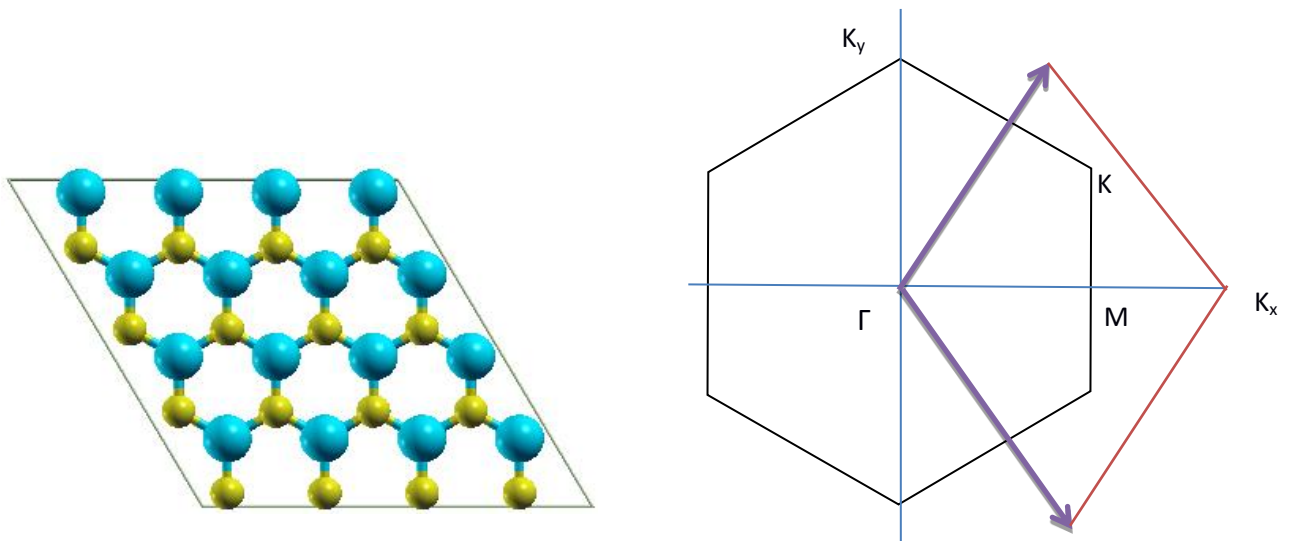


Fig. 4.1: Optimized atomistic model of 2D-SiC with unit cell outlined as dashed line. (b) The corresponding first Brillouin zone and high symmetry points.

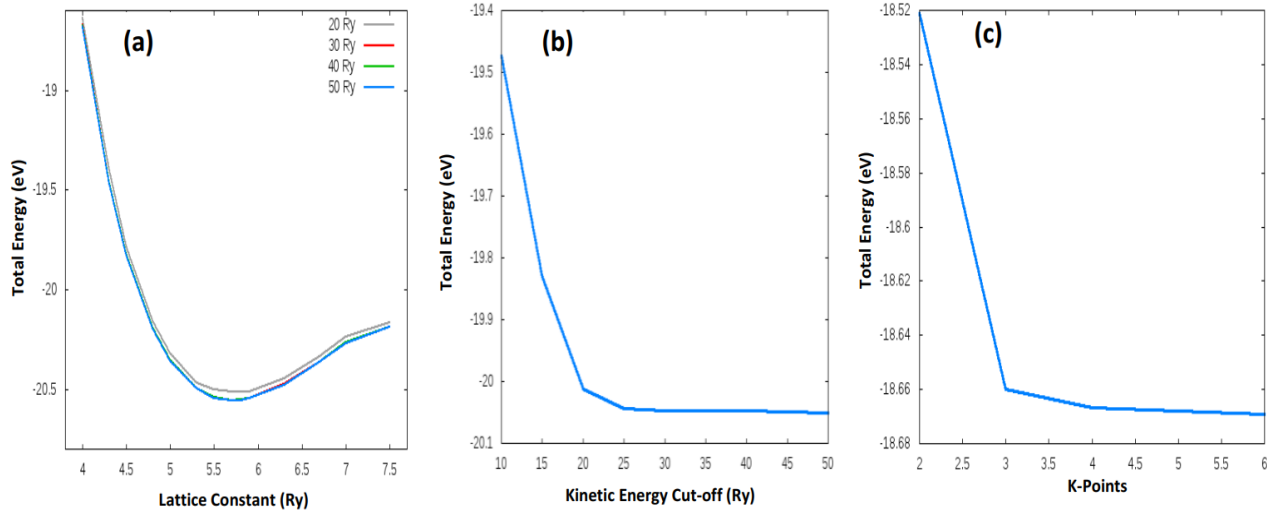


Fig. 4.2: Total energy per unit cell of 2D-SiC with the variation of (a) lattice constant (b) kinetic energy cut-off and (c) K -points.

Since relative stability needs a good k -point sampling, it is observed from Fig. 2(c) that k -point mesh of $4 \times 4 \times 1$ is sufficient for our structure. From the convergence of the total energy, it is found that a kinetic energy cutoff of 30-50 Ry is adequate for hexagonal 2D SiC structure.

4.3 Electronic properties without spin orbiting coupling (SOC) effect

After obtaining the stable system, we explore the electronic properties of this favorable structure. Firstly, the electronic band structure has been calculated self-consistently by using the LDA. Fig. 4.3 presents the electronic band structure and density of states from LDA calculations. As shown in Fig. 4(a), both the valence band maximum (VBM) and conduction band minimum (CBM) have been located at the K -point. Consequently, the energy bands estimated by our calculation guesses a direct band gap $E_k = 2.71$ eV. The Fermi level (dotted line in Fig. 4.3) is separated by two bands consisting of hybridized π and π^* orbitals from Si and C atoms. For better understanding the contribution of individual elements in the electronic structure, the projected density of states (PDOS) has been calculated. The 2D-SiC is produced by the sp^2 orbital hybridization combining σ -bonds and π -bonds. The σ -bond is formed by the silicon (Si-2s, $3p_x, 3p_y$) and carbon (C-1s, $2p_x, 2p_y$) electrons and the π -bond is generated by the Si- $3p_z$ and C- $2p_z$ electrons. The conduction and valence band edges at the K point are constructed by the π and π^* -bands, which is formed due to the bonding and anti-bonding combination of Si- $3p_z$ and C- $2p_z$ orbitals. We show the contribution of the electrons of two elements in Fig. 4.4. The peaks of the

PDOS in the conduction band (2 to 6 eV) as well as in the valence band (-5 to 0.8 eV) are dominantly contributed by carbon. The peaks of the PDOS in the conduction band (2 to 6 eV) as well as in the valence band (-5 to -1.4 eV) are dominantly contributed by silicon. The lowest conduction band forms mainly from the Si-3p orbital with a small contribution from the C-2p orbitals. The highest valence band forms from the C-2p orbital with a small contribution from the Si-3p and Si-2s orbits.

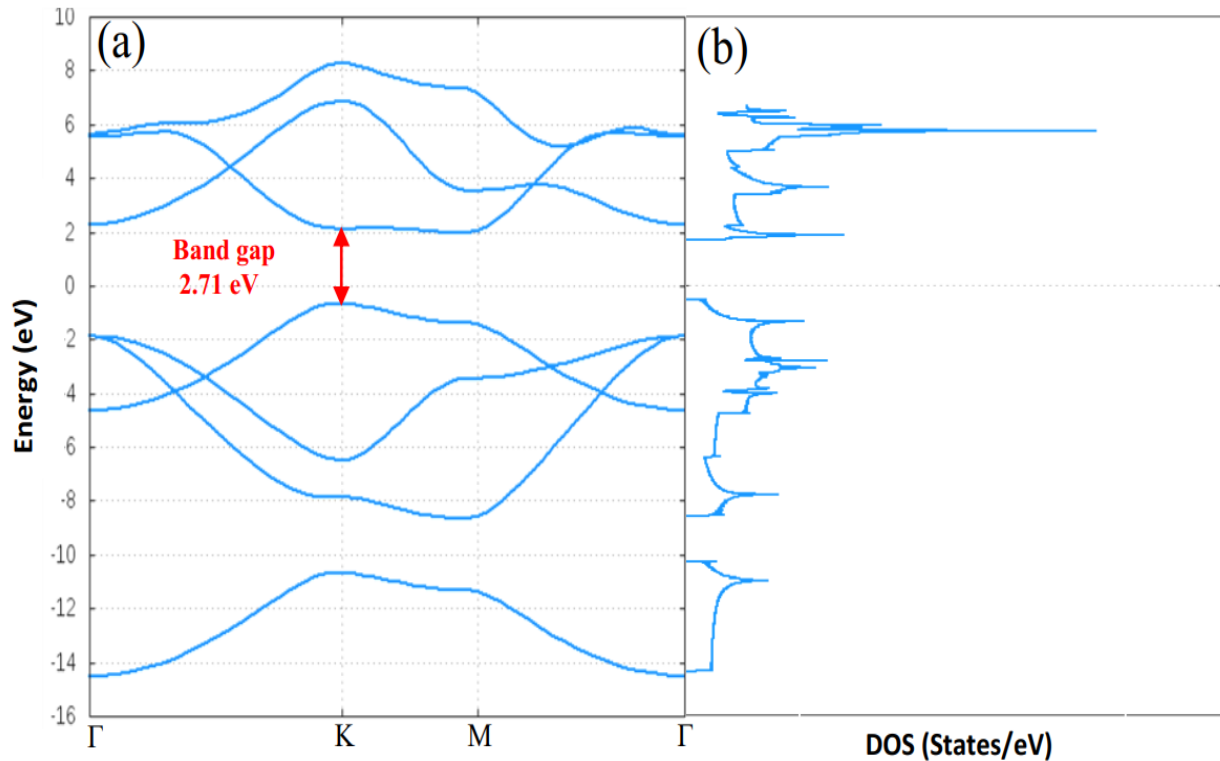


Fig. 4.3: (a) Electronic band structure and (b) density of states (DOS) of 2D-SiC without considering the SOC. The Fermi level is set to zero. A direct energy band gap at *K*-point is shown by the red arrow.

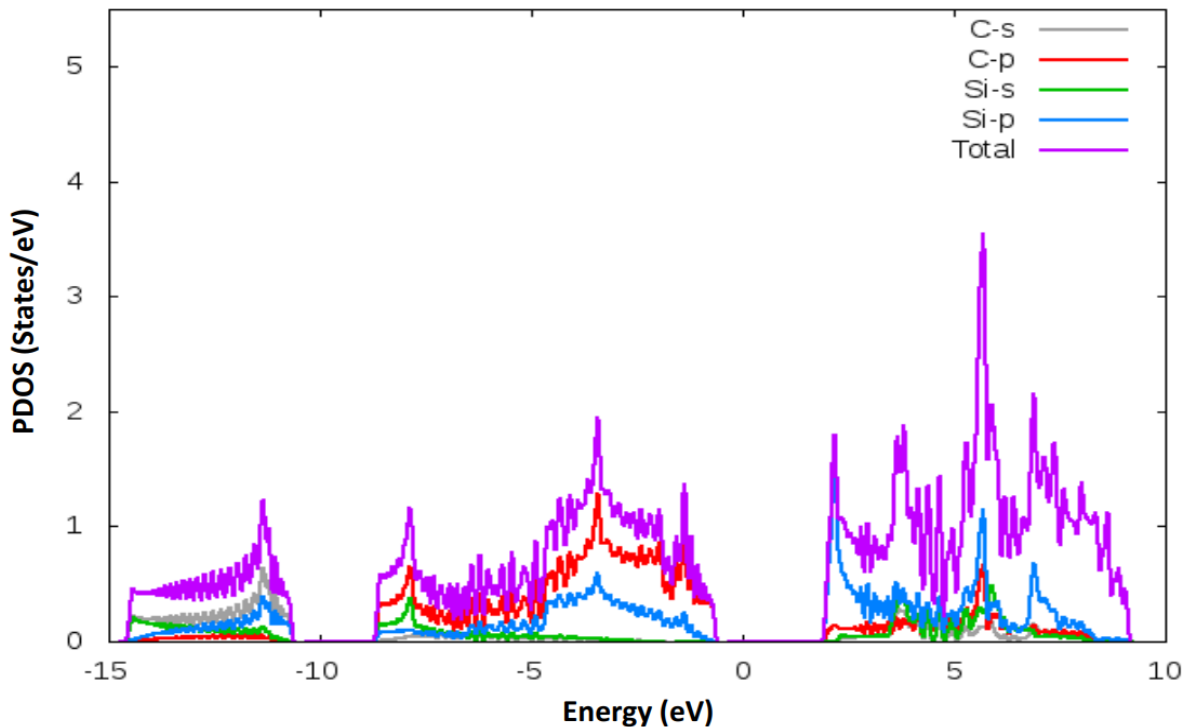


Fig. 4.4: Projected density of state (PDOS) of 2D-SiC with separate contributions from each orbital atoms without SOC.

4.4 Electronic properties with spin orbiting coupling (SOC) effect

The spin orbital interaction plays a crucial role in the electronic structure of the solid. SOC is an important element to quantitatively correct the band structures of solids. We incorporate the SOC effect in the calculations diagonalizing the total Hamiltonian containing the spin-orbit interaction and the self consistently determined Kohn-Sham Hamiltonian. Owing to the electromagnetic interaction between the spin and the magnetic field, the effect of SOC has been developed in the material. The electron energy levels lead to a shift because of this interaction happens for protons and neutrons stirring inside the nucleus. Earlier works on honeycomb graphene and related structures show that the SOC effect increases the bandgap although bandgap decreases in some structure. 2D stanene has a zero band gap without SOC, however, 0.1 eV SOC induced band gap has been reported in the literature [78]. Owing to the SOC, a splitting of the valence band is occurred. A large spin-orbit splitting in the valence band of transition

metal dichalcogenide is observed owing to the relativistic effects induced by heavy atomic core [79].

Generally, the splitting of bands can be understood from the total angular momentum created by the interaction between the spin angular momentum and orbital angular momentum. The total spin angular momentum s and the total orbital angular momentum l are merged and developed the ls coupling. The total angular momentum j can be developed by this ls coupling in the form $(l+s)$, $(l+s-1)$, ... $(l-s)$. The values of j are ranging from $|l-s|$ to $|l+s|$. For s orbital $l=0$, $j=1/2$ and for p orbital $l=1$, $j=1/2$ and $j=3/2$, where $s=+1/2$ and $-1/2$. This coupling has an intuitive effect on the energy band structure of materials. For example, it is found in GaAs semiconductor that the top of the valence bands is a p-like (i.e., orbital angular momentum $l=1$) while no SOC is considered. However, the electronic states with SOC gives the total angular momentum $j=3/2$ and $j=1/2$. Hence, an energy gap is generated between these new $j=3/2$ and $j=1/2$ states, which is so called as the SOC gap.

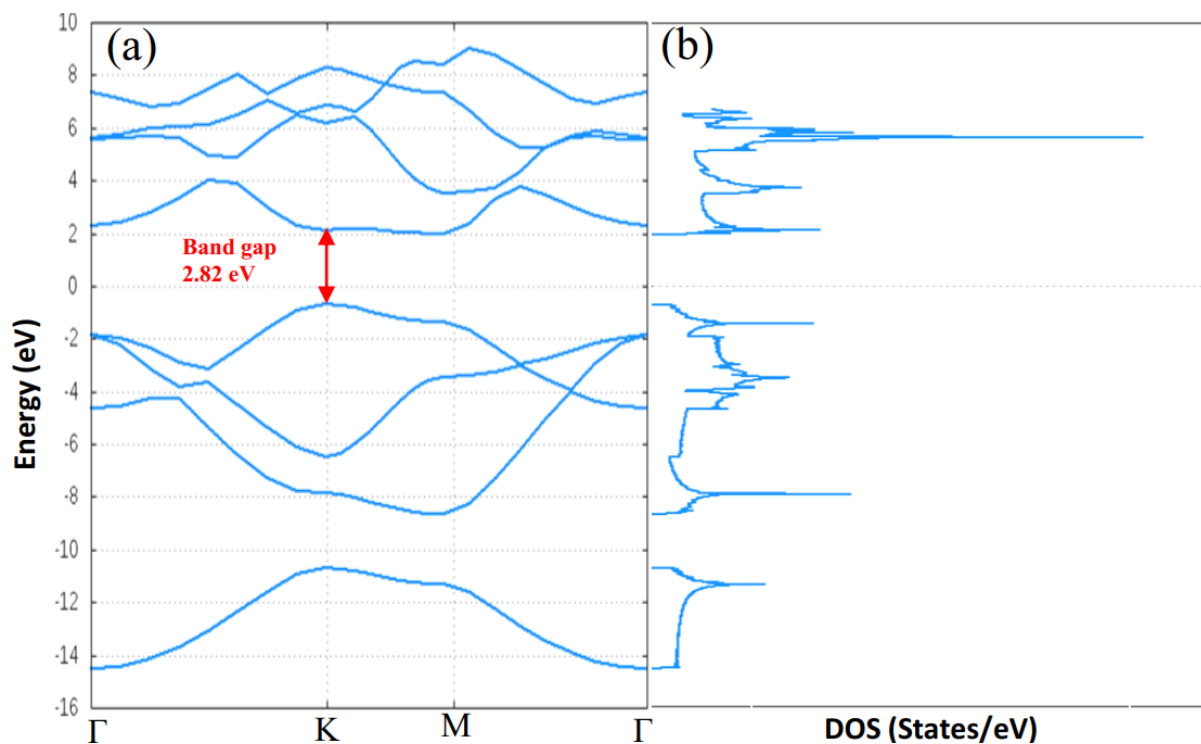


Fig. 4.5: (a) Electronic band structure and (b) DOS of 2D-SiC with SOC. The band structure changes and increases the energy gap at the K -point due to the SOC effect.

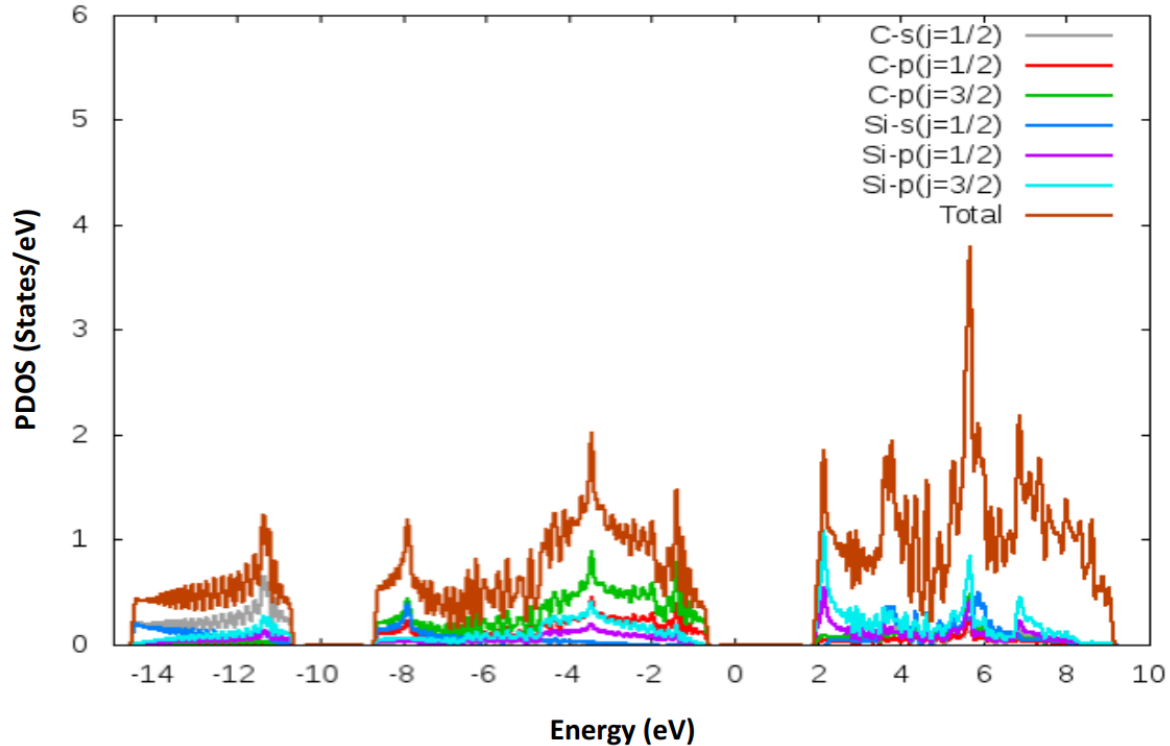


Fig. 4.6: PDOS of 2D-SiC with separate contributions from each orbital atoms. The p-orbital splits into two new branches due to the SOC

In 2D SiC, splitting occurs in both the valence and conduction bands and thus the energy gap is increased while considering the SOC. Fig. 4.5 depicts the energy band structure and electronic DOS incorporating the SOC effect. At the K -point of the BZ an energy gap of ~ 2.827 eV is determined. We observe that considering the SOC leads to a band gap increase of 117 meV. Fig. 4.6 shows the PDOS taking into account the SOC effect. While including the SOC in the PDOS, the contribution of electron in conduction and valence band is different as for no SOC effect. Near the Fermi level, the contribution of Si is mainly in the conduction band and the contribution of carbon is mainly in the valence band. The peaks of the PDOS in the conduction band (5 to 7 eV) as well as in the valence band (-5 to 0.9 eV) are dominantly contributed by C atom. The peaks of the PDOS in the conduction band (2 to 6 eV) as well as in the valence band (-5 to -2 eV) are dominantly contributed by Si atom. However, in case of both Si and C, s orbitals have only one branch of angular momentum, $j=1/2$ and p orbitals have two branches of angular momentum $j=1/2$ and $j=3/2$. Therefore, we obtain two more branches owing to these new angular momentums as shown in Fig. 7. Due to the contribution of C atoms, the peaks become apparent in the conduction band (2 to 4 eV) as well as in the valence band (-5 to 0 eV) for both angular

momentums $j=1/2$ and $j=3/2$. Also due to the contribution of Si atoms, the peaks are appeared in the conduction band (2 to 4 eV) as well as in the valence band (-4 to 0 eV) for both angular momentums $j=1/2$ and $j=3/2$.

4.5 Phonon properties

Probing the lattice vibrational modes offers a dependable check for the structural stability. The imaginary frequency of phonon modes indicates the dynamic instability of a crystal structure. The frequency, $\omega(\mathbf{k})$ attained from the dynamical matrix of the unstable structure becomes negative providing the imaginary frequency due to the existence of instability related to a phonon mode in the \mathbf{k} point BZ. The imaginary frequency mode cannot produce the restoring force to perform atomic vibration and thus the system is exposed to disappear from its original geometry. Phonon properties also play a major role in many of the physical properties of condensed matter, like thermal conductivity and electrical conductivity.

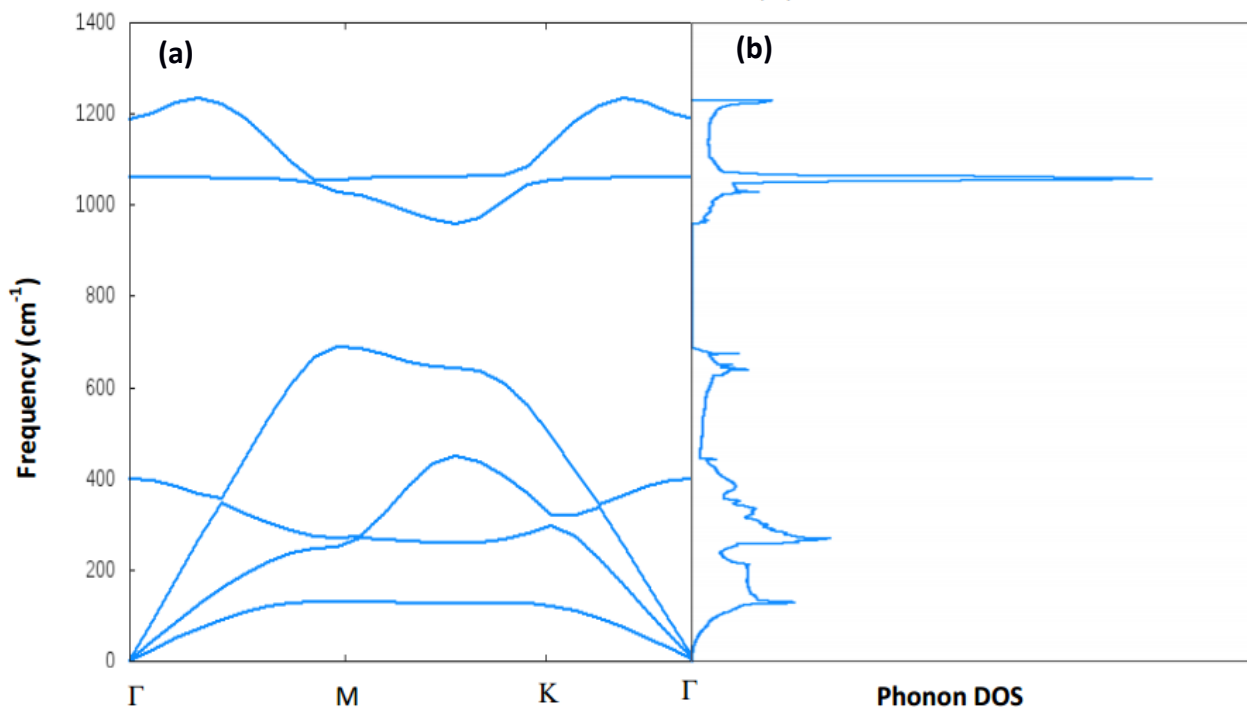


Fig. 4.7: (a) Phonon dispersion relationship with Ultrasoft pseudopotential using first principle density function theory, and (b) Corresponding Phonon Density of State of 2D-SiC.

Furthermore, the phonon is used to analysis of Raman active modes, disorder of the sample, the tension and compression state, the number of graphitic layers, interlayer coupling, oxidation, thermal properties and more. Thus, the study of phonons is an important part of condensed matter physics. We have carried out the phonon calculations using DFT to further test the stability of the structure.

In Fig. 4.7, we present the calculated phonon dispersion relation and corresponding density of states of the honeycomb structure of the 2D-SiC sheet. The phonon spectrum shows no negative frequency implying the stable phase of the structure without any dynamical instability. The longitudinal acoustic (LA), transverse acoustic (TA), and flexural or out of plane acoustic (ZA) modes are the three acoustic modes. These are the lowest frequencies mode at the zone center or Γ point. However, the higher frequencies mode is longitudinal optical (LO), transverse optical (TO), and out of plane optical (ZO) modes. The all frequencies of the phonon modes are below the 1190cm^{-1} . There is a large phonon band gap lies between 700 and 960cm^{-1} and this value is 260cm^{-1} . The corresponding total phonon density of states (PHDOS) confirms the phonon dispersion outcome, which is depicted in Fig. 3(b).

4.6 Raman and infrared (IR) spectra

Raman and infrared (IR) spectra both are the invaluable spectroscopic technique to detect the vibrational properties. A phonon will be Raman or IR active if it causes a change in polarizability or permanent dipole moment of the materials, respectively. To characterize the graphene and related 2D honeycomb materials, especially Raman spectra has been used as an important characterization tool in the last few years. The various peaks of the Raman and infrared spectra can be deduced from various phonon modes of the solids. A completely C or Si based 2D systems i.e. graphene or silicene shows a Raman peak near 1600cm^{-1} and 570cm^{-1} , this peak is so called the G peak and come from the Γ point in-plane transversal optical (iTO) and in-plane longitudinal optical (iLO) phonon modes. With the analogy of graphene and silicene, we can obtain the Raman active modes of the 2D-SiC sheet from the phonon dispersion relation.

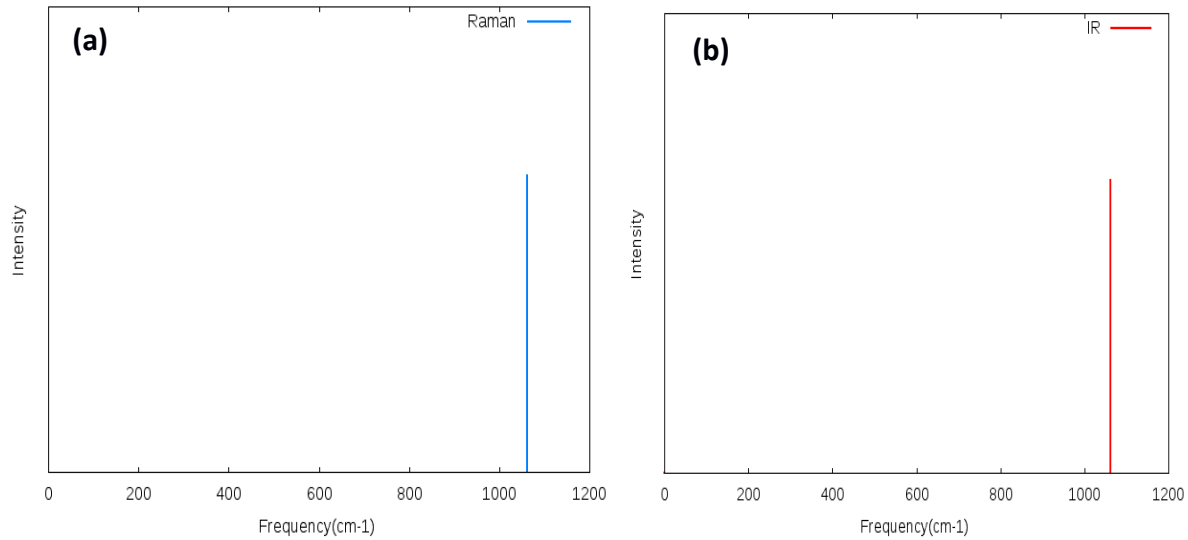


Fig. 4.8: (a) Raman and (b) IR Spectra of 2D-SiC.

Our calculated Raman spectrum shows a sharp peak at 1045 cm^{-1} as exhibited in Fig.5. Although Γ -point iTO and iLO mode phonons are degenerate for graphene and silicene, these modes are nondegenerate for SiC sheet. The energy of the Raman active mode has been evaluated at the transverse optical branch at Γ and the value of phonon mode is 1045 cm^{-1} .

4.7 Thermal properties

The Helmholtz free energy is an important parameter to determine the stability of a structure. In thermodynamics, the Helmholtz free energy is a thermodynamic potential that measures the useful work obtainable from a closed thermodynamic system at a constant temperature and volume. A structure with a more negative value of Helmholtz free energy will be considered more stable. We calculated the Helmholtz free energy F_A , at constant volume of 2D-SiC monolayers as a function of temperature, as shown in Fig. 4.9. We notice that the Helmholtz free energy decreases monotonically with respect to temperature, opposed to trends of heat capacity. At the 0 K temperature is attributed to the existence of zero-point motion and calculated free energy at absolute zero is 0.015 kJ/mol. The 2D-SiC is a stable structure because of a negative value of Helmholtz free energy with increasing the temperature. Furthermore, at a certain temperature, the Helmholtz energy is minimized at equilibrium.

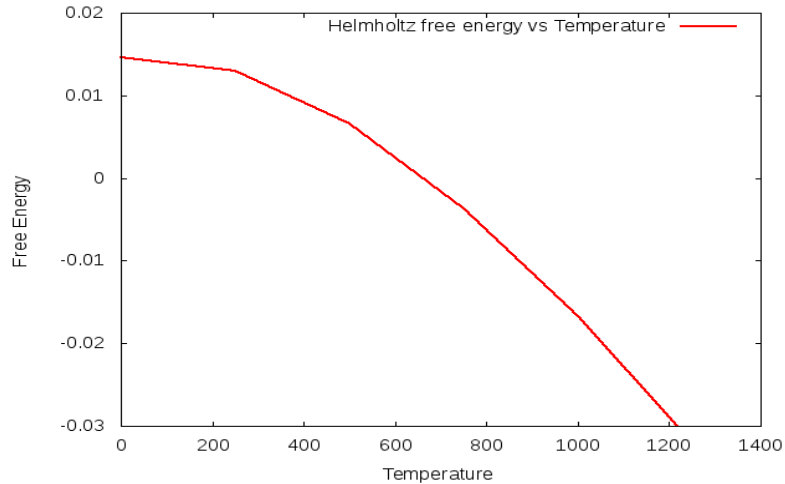


Fig. 4.9. The Helmholtz free energy F_A at constant volume of 2D-SiC monolayers are calculated as a function of temperature with harmonic approximation.

4.8 Effect of Vacancy defects on 2D-SiC

The effects of Si and C vacancies in periodically repeating (4×4) supercells have shown in figure 4.10. The size of supercell is optimized to allow negligible defect interaction between adjacent cells. A (4×4) supercell led to rather vacancy defect bands which are suitable for our purpose, but allowed us to carry out numerical calculations.

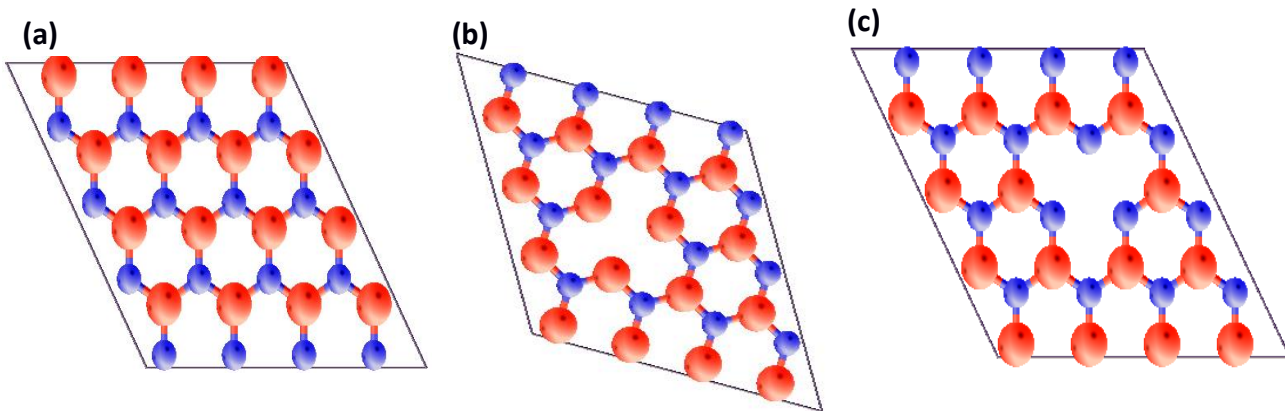


Fig. 4.10: (a) Atomic structure of 2D-SiC (4×4 supercell). (b) Single carbon vacancy, and (c) Single silicon vacancy of 2D-SiC (Si is red color and carbon is blue color).

4.8.1 Carbon and silicon vacancy effects on electronic properties

Generally, a single vacancy is the simplest intrinsic defect in a crystal. The vacancy defect has been observed through transmission electron microscopy (TEM) [80] and scanning tunneling microscopy (STM) [81]. When an atom is removed, two scenarios are possible: either the disrupted bonds remain as dangling bonds or the structure undergoes a bond reconstruction through a Jahn-Teller rearrangement and in three-dimensional (3D) semiconductors, it finds a localized state and deep gap levels. Moreover, it is found in graphene that defects can change the interatomic bond length. They also change the type of the hybrid trajectories of the partial carbon atoms. The changes of bond length and orbital are responsible for the major change of electrical properties of graphene. Point defects and single vacancy defects of graphene form an electron scattering center on the surface. This center affects electron transfer, resulting in a decrease in the conductivity of graphene.

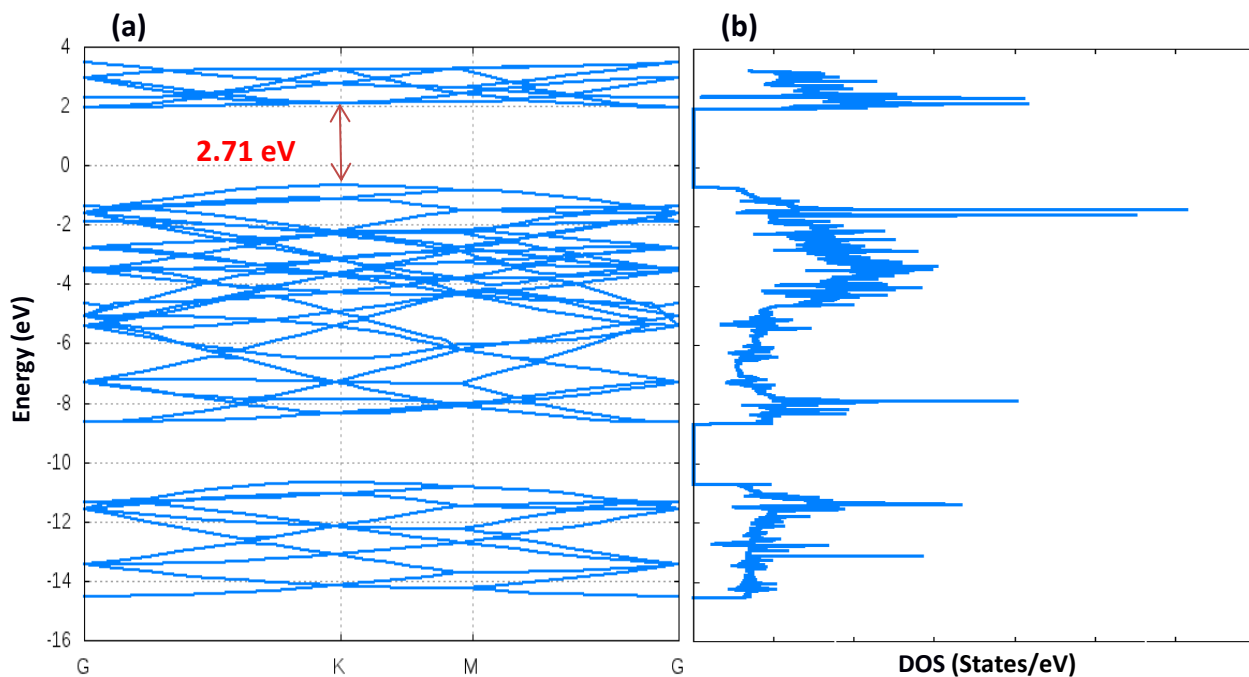


Fig. 4.11: (a) Electronic band structure of 2D-SiC (4×4 supercell) using DFT.(b)Corresponding density of state (DOS)

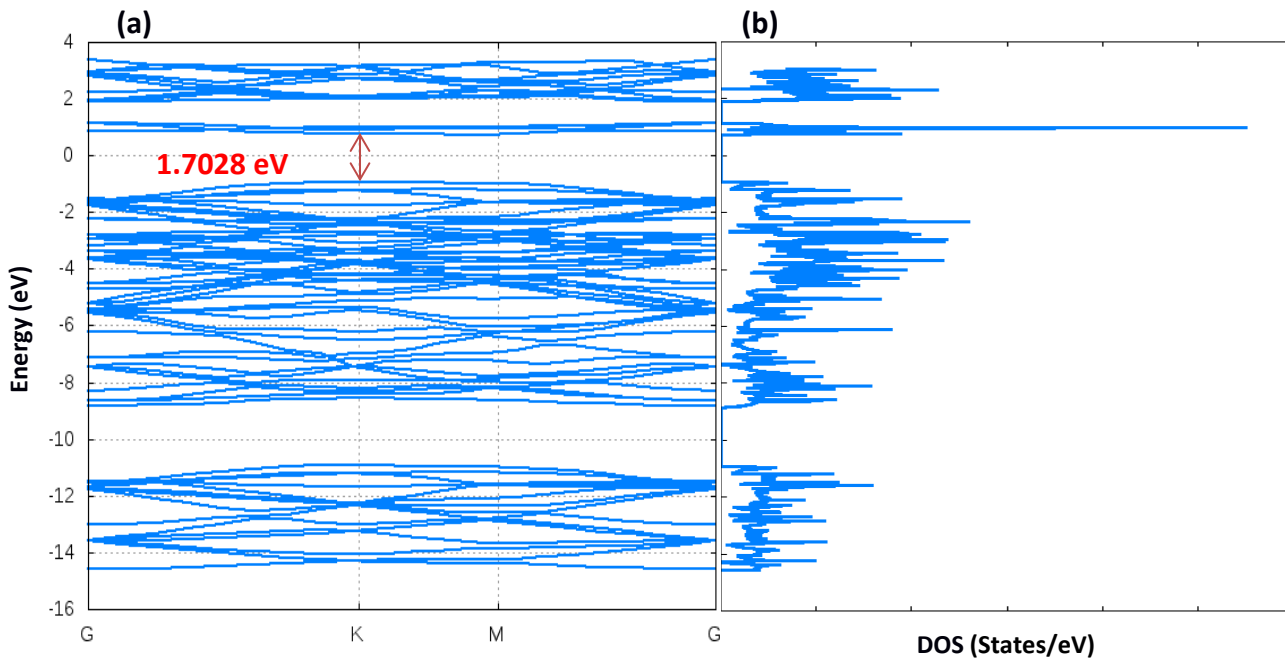


Fig. 4.12: (a) Electronic band structure of 2D-SiC with carbon vacancy defect (4×4 supercell). (b) DOS.

The vacancy defect has a significant effect on the electronic properties of two-dimensional (2D) materials. The novel protocol has improved the visible photocatalytic activity of modified ZnO nanostructures through the promotion of oxygen vacancies, which resulted in band gap narrowing of the ZnO nanostructure ($E_g = 3.05$ eV) from wide band gap of ZnO ($E_g = 3.24$ eV) [82]. GaN is a direct wide band gap semiconductor material with energy gap of 1.66 eV and with considering the Ga and N vacancy the bandgap increase to 2.30 eV and 1.97 eV respectively [83]. Thus, investigating the effect of vacancy on the electronic properties of the newly discovered 2D-SiC monolayer is a great interest for future spintronic devices. The band structure of the pure 2D-SiC is depicted in figure 4.11. The valence band maximum and conduction band minimum of pure 2D-SiC (4×4) supercell is located in the K-point of Brillouin zone. The results indicate that 2D-SiC is a direct wide bandgap semiconductor material with energy gap of 2.71 eV. It can be perceived from figure 4.12 and figure 4.13 that the numbers of the valence band and conduction band significantly increase in 2D-SiC for both carbon (V_C) and silicon (V_{Si}) vacancy as well as the band gap is decreased than that of the pure 2D-SiC. The band gaps of 2D-SiC: V_C and 2D-SiC: V_{Si} have been decreased to 1.7028 eV and 2.4664 eV, respectively.

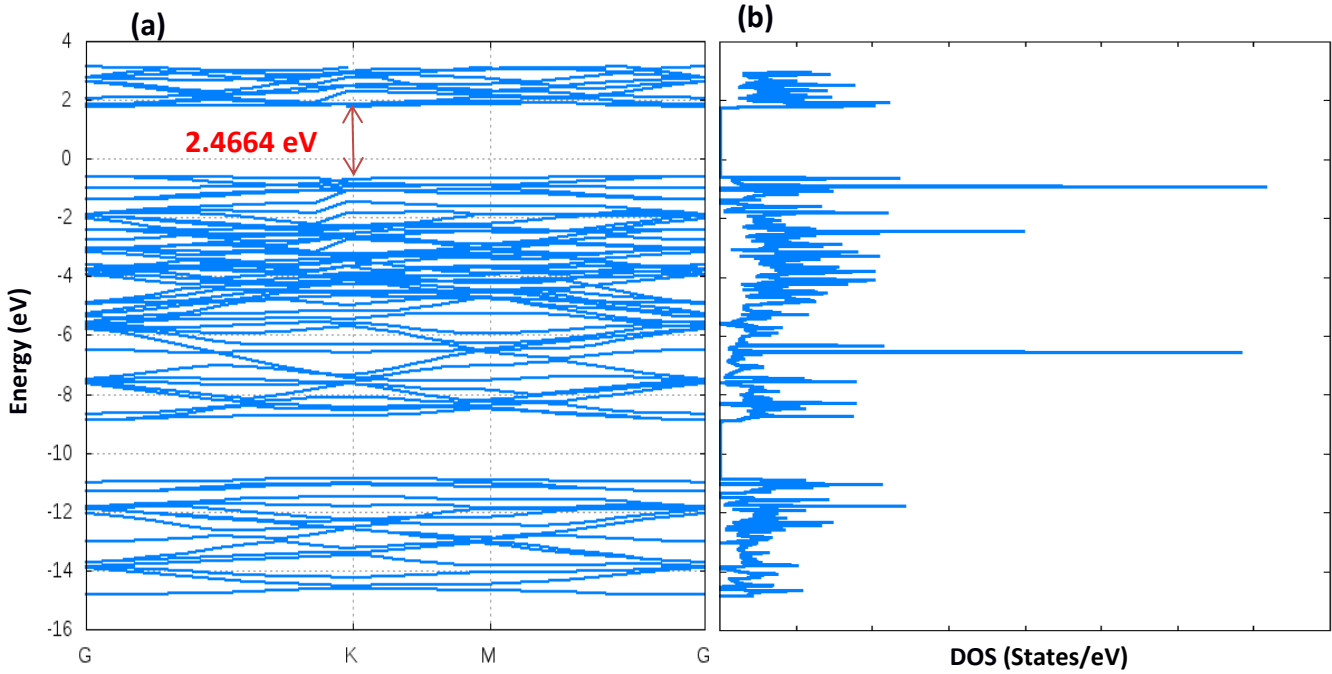


Fig. 4.13: Electronic band structure of 2D-SiC with silicon vacancy defect (4×4 supercell) (b) DOS

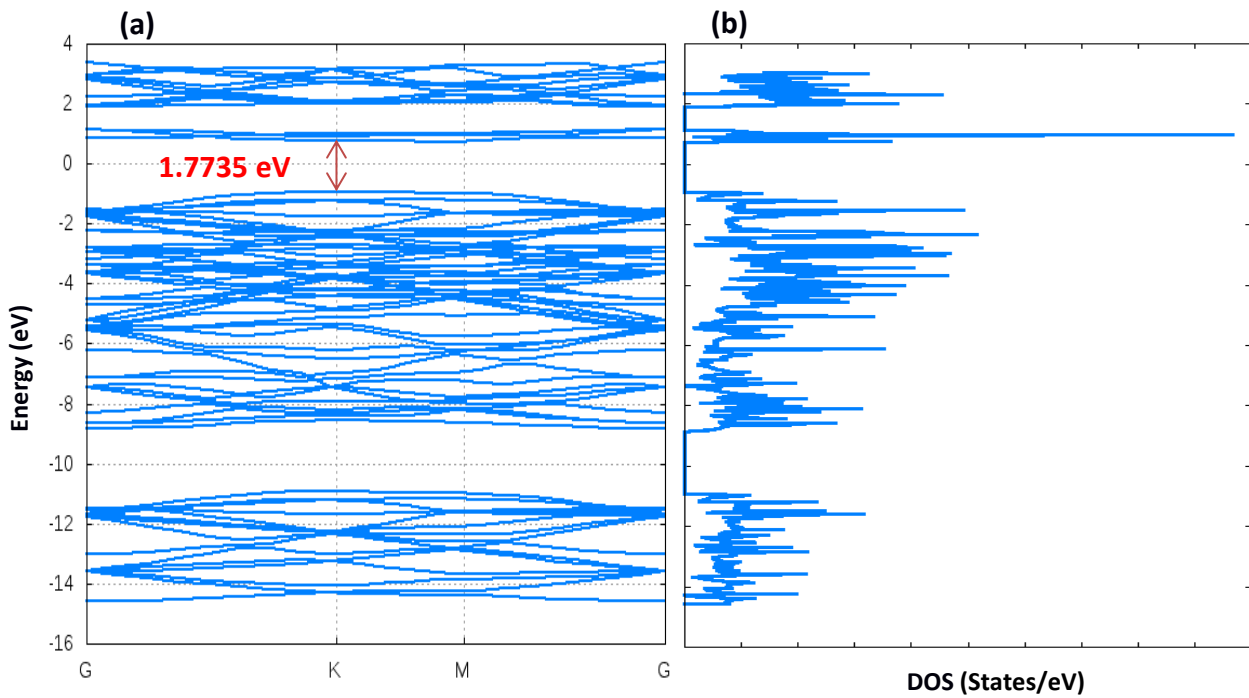


Fig. 4.14: Electronic band structure of 2D-SiC with carbon vacancy defect, including SOC effect (4×4 supercell) .

4.8.2 Combined vacancy and SOC effects on electronic properties

The electronic properties of material has been changed due to SOC effect for pure 2D-SiC which was presented in Fig. 4.5 for the unit cell. The electronic properties have also modified owing to the combined effect of SOC and defects of 2D-SiC. Spin-orbit coupling (SOC) establishes itself by lifting the spin degeneracy in the electronic structures, such as the magnetic anisotropy in magnetic systems and the band splitting of surface states when the systems lack the inversion symmetry. The band structure of graphene, MoS₂ and metal surfaces have been changed due to SOC effect for both pure and defective structure [84]. There is no study showed on the SOC effect on the electronic structure of defective 2D-SiC. Hence, including SOC effect with single vacancy defect of carbon and silicon in 2D-SiC, the electronic band structure has been calculated here. When it has been considered of SOC on the carbon vacancy defective structure of 2D-SiC, the bandgap is turn to 1.7735 eV from 1.7028 eV which depicted in figure 4.14. Furthermore, when it has been considered of SOC on the silicon vacancy defective structure of 2D-SiC, the bandgap is changed to 2.526 eV from 2.4464 eV, which illustrated in Fig. 4. 15.

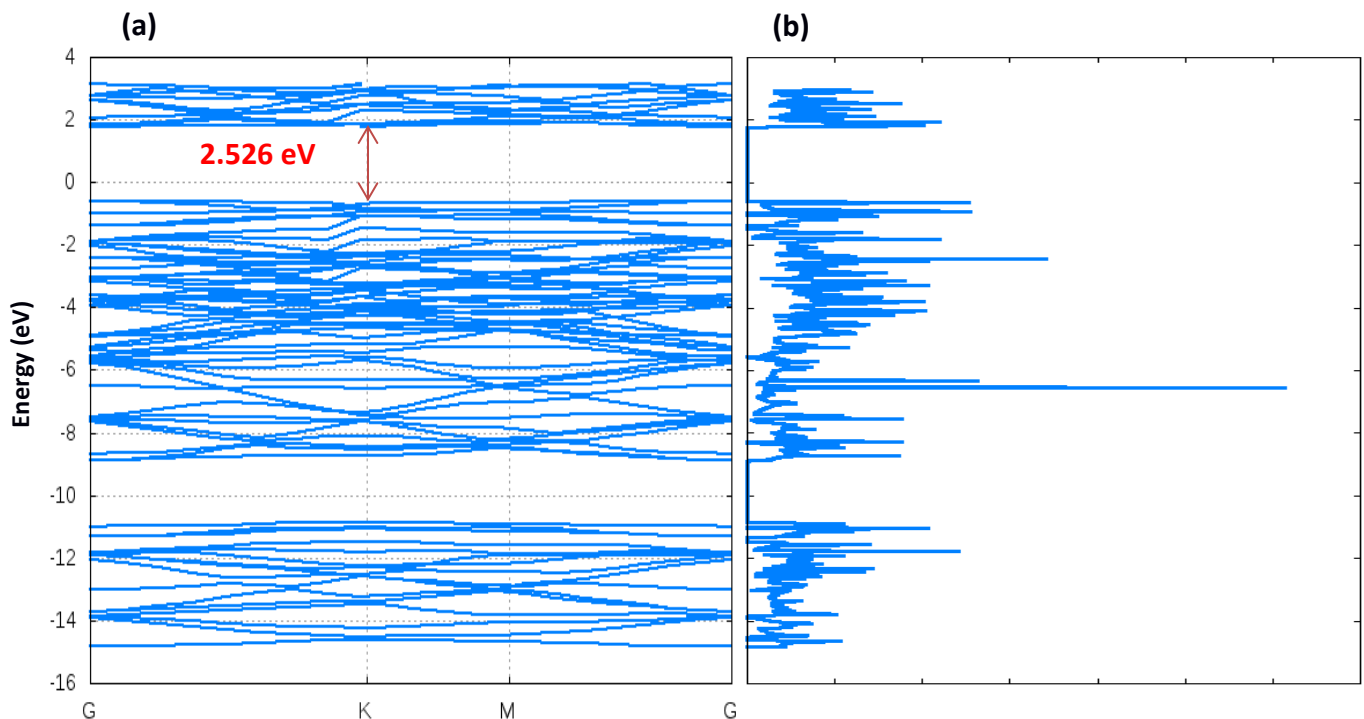


Fig. 4.15: Electronic band structure of 2D-SiC with silicon vacancy defect, including SOC effect (4×4 supercell).

Chapter

V

SUMMARY AND OUTLOOK

Chapter at a Glance

- | | |
|---------------|-------------|
| • Conclusion | Section 5.1 |
| • Future Work | Section 5.2 |

5.1 Conclusion

In this thesis, the detailed structural, electronic, and vibrational properties of the 2D-SiC nanomaterial have been systematically investigated by the first principle DFT calculations. It has graphene-like honeycomb lattice which have superior structural and dynamical stability. The structural stability has checked by the calculation of minimum energy with variation of energy with respect to lattice constant, kinetic energy cut-off and K-points respectively. The electronic band structure and density of states presents that the both the valence band maximum (VBM) and conduction band minimum (CBM) have been located at the K-point and thus develop a direct band gap 2.71 eV. The Fermi level is separated by two bands consisting of hybridized π and π^* orbitals from Si and C atoms. The 2D-SiC have been produced by the sp^2 orbital hybridization combining σ -bonds and π -bonds. The σ -bond has been formed by the silicon (Si-2s, 3p_x,3p_y) and carbon (C-1s,2p_x,2p_y) electrons and the π -bond has been generated by the Si-3p_z and C-2p_z electrons. The calculated projected density of states (PDOSs) have exposed that the conduction and valence band edges at the K point have been constructed by the π and π^* -bands, which are formed due to the bonding and anti-bonding combination of Si-3p_z and C-2p_z orbitals.

The negative frequencies are not present in the phonon dispersion relation which indicate that the 2D-SiC structure is dynamically stable. The large phonon band gap has been produced which lies between 700 and 960 cm⁻¹ and this value is 260 cm⁻¹. From the phonon dispersion relation, the phonon density of state, Raman spectra and thermal properties have been also calculated. The energy of the Raman active mode has been estimated at the transverse optical branch at Γ and the value of phonon mode is 1045 cm⁻¹. We have also systematically explored the effects of SOC on the electronic structure of 2D-SiC using the first-principle calculations within the framework of DFT study. Our DFT calculations on the electronic energy band structure and DOS of 2D-SiC have shown that the energy gap near the K-point is ~2.71 eV, whereas the energy gap increases to ~2.827 eV while considering the SOC effect. It is observed that the electronic states with SOC induces two new branches in PDOS owing to the total angular momentums $j = 3/2$ and $j = 1/2$, which generates an energy gap in the band structure. Furthermore, the band gaps of 2D-SiC with carbon and silicon vacancy decrease to 1.7028 eV and 2.4664 eV, respectively from the direct bandgap 2.71eV. However, the effects of SOC on the carbon and silicon vacancy type 2D-SiC structures show the increasing of bandgap from 1.7028

eV to 1.7735 eV and from 2.4664 eV to 2.526 eV, respectively. These results are very much important to explore the fascinating physics of spin-orbit Dirac fermions and potential applications of 2D-SiC in optoelectronics and spintronic devices.

5.2 Future work

The first principle DFT technique described in this dissertation has proven to accurately describe the structural, electronic and vibrational properties of 2D-SiC. It has been calculated the electronic properties of 2D-SiC including vacancy defect with considering SOC effect. At the same time, there have been several important issues in the field that remain to be addressed. This simulation method developed in this dissertation can be extended to this material for vibrational properties of vacancy defected structure. It will be also calculated to electron-phonon coupling effect, thermal conductivity of 2D-SiC structure both pure and defected.

Bibliography

- [1] G. Pens, F. O, T. Frank, M. Krieger, S. Reshavon, F. Schmid and M. Weidner, "SiC material Properties," *International Journal of High Speed Electronics and Systems*, vol. 15, pp. 705-745, 2005.
- [2] S. E. Saddow and A. Agarwal (eds), "Advances in silicon carbide processing and applications," Artech House, Norwood (2004).
- [3] H. Morkoc, S. Strite, GB. Gao, ME. Lin, B. Sverdlov and M. Burns, "Large-band-gap SiC, III–V nitride, and II–VI ZnSe-based semiconductor," *J Appl Phys*, vol. 76, pp. 1363-98, 2015.
- [4] Y. Goldberg, ME. Levinshtein, SL. Rumyantsev and MS. Shur, "Properties of advanced semiconductor materials GaN, AlN, SiC, BN, SiC, SiGe," John Wiley & Sons, Inc., vol 43, pp. 93-148, 2001.
- [5] R. Presser and KG. Nickel, "Silica on silicon carbide," *Crit Rev Solid State*; vol. 33 pp. 1-99, 2008.
- [6] Philip G. Neudeck "Progress towards high temperature, high power SiC devices", *Institute of Physics Conf.: Compound Semiconductors* vol. 141, pp. 1-6, 1994.
- [7] P. A. Ivanov and V. E. Chelnokov, "Recent developments in SiC single-crystal electronics," *Semicond. Sci. Technol.*, vol. 7, pp. 863-880, 1992.
- [8] G. L. Harris, "Properties of Silicon Carbide," *INSPEC Institution of Electrical Engineers*, London, 1995.
- [9] S. S. Lin., "Light Emitting Two-Dimensiona Ultrathin Silicon Carbide," *J. Phys. Chem. C*, vol. 116, pp. 3951-3955, 2012.
- [10] N. G. Hingorani and K. E. Stahlkopf *Scientific American*, vol. 269 (5), pp. 78-85, 1993.
- [11] Y. M. Tairov and V. F. Tsvetkov, *J. Cryst. Growth*, vol. 43, pp. 209-212, 1978.
- [12] X. Lin, S. Lin, Y. Xu, A. A. Hakro, T. Hasan, B. Zhang, B. Yu, J. Luo, E. Liad and H. Chena "Ab initio study of electronic and optical behavior of two dimensional silicon carbide" *J. Mater. Chem. C*, vol. 1, pp. 2131 -2135, 2013.
- [13] P. A. Ivanov and V. E. Chelnokov, "Recent developments in SiC single-crystal electronics ," *Semicond. Sci. Technol.*, vol. 7, pp. 863-880, 1992.

- [14] S. S. Lin., "Light Emitting Two-Dimensional Ultrathin Silicon Carbide," *J. Phys. Chem. C*, vol. 116, pp. 3951-3955, 2012.
- [15] "Silicon carbide Power devices: Advanced gate driving techniques", AgileSwitch SiC Product Overview January 2016.
- [16] T. P. Chow and R. Tyagi, "Wide bandgap compound semiconductors for superior high-voltage unipolar power devices," *IEEE Trans. Electron Devices*, vol. 41, pp. 1481–1483, Aug. 1994.
- [17] M. Bhatnagar and B. J. Baliga, "Comparison of 6H-SiC, 3C-SiC, and Si for power devices," *IEEE Trans. Electron Devices*, vol. 40, pp. 645–655, Mar. 1993.
- [18] B. J. Baliga, "Power semiconductor device figure of merit for high-frequency applications," *IEEE Electron Device Lett.*, vol. 10, pp. 455–457, Oct. 1989.
- [19] "Changing markets are served by gate driver ICs", ROHM Semiconductor GmbH, may 2015.
- [20] Q. Huy Ta, L. Zhao, D. Pohl, J. Pang, B. Trzebicka, B. Rellinghaus, D. Pribat, T. Gemming, Z. Liu, A. Bachmatiuk and M. H. Rummeli, "Graphene-Like ZnO: A Mini Review," *Crystals*, vol 6, pp. 100-105, 2016.
- [21] Lee, C., "Measurement of the Elastic Properties and Intrinsic Strength of Monolayer Graphene" *Science*, vol. 321, pp. 385, 2008.
- [22] K. S. Novoselov, Z. Jiang, Y. Zhang, S. V. Morozov, H. L. Stormer, U. Zeitler, J. C. Maan, G. S. Boebinger, P. Kim and A. K. Geim, "Room-Temperature Quantum Hall Effect in Graphene Science," *Nature*, vol. 315, pp. 1379 –1379, 2007.
- [23] H. C. Hsueh, G. Y. Guo and S. G. Louie, "Excitonic effects in the optical properties of a SiC sheet and nanotubes," *Phys. Rev. B: Condens. Matter Mater. Phys.*, vol. 84, pp. 404-408, 2011.
- [24] X. Lin, S. Lin, Y. Xu, A. A. Hakro, T. Hasan, B. Zhang, B. Yu, J. Luo, E. Liad and H. Chena "Ab initio study of electronic and optical behavior of two dimensional silicon carbide" *J. Mater. Chem. C*, vol. 1, pp. 2131 -2135, 2013.
- [25] E. Fortin, S. Fafard, and A. Mysyrowicz, "Exciton transport in Cu₂O: Evidence for excitonic superfluidity", *Phys. Rev. Lett.*, vol. 70, pp. 3951-3952, 1993.

- [26] S. Lin, S. Zhang, X. Li, W. Xu, X. Pi, X. Liu, E. Wang, H. Wu and H. Chen, "Quasi-Two-Dimensional SiC and SiC₂: Interaction of Silicon and Carbon at Atomic Thin Lattice Plane," *J. Phys. Chem. C*, vol. 119, pp. 19772-19779, 2015.
- [27] T. Susi, V. Skakalov, A. Mittelberger, P. Kotrusz, M. Hulman, T. J. Pennycook, C. Mangler, J. Kotakoski and J. C. Meyer, "Computational insights and the observation of SiC nanograin assembly: towards 2D silicon carbide," *Scientific reports*, vol. 7, pp. 4399, 2017.
- [28] G. Pens, F. Ciobanu, T. Frank, M. Krieger, S. Reshavon, F. Schmid and M. Weidner, "SiC material Properties," *International Journal of High Speed Electronics and Systems*, vol. 15, pp. 705-745, 2005.
- [29] Z. Shi, Z. Zhang, A. Kutana, and B. I. Yakobson, "Predicting Two-Dimensional Silicon Carbide Monolayers," *ACS Nano*, vol. 9, pp. 9802-9809, 2016.
- [30] Y. Li, F. Li, Z. Zhou and Z. Chen, "Two-Dimensional Cu₂Si Monolayer with Planar Hexacoordinate Copper and Silicon Bonding," *J. Am. Chem. Soc.*, vol. 133, pp. 900-908, 2010.
- [31] R. J. Elliott, "Theory of the Effect of Spin-Orbit Coupling on Magnetic Resonance in Some Semiconductors", *Phys. Rev.* vol. 96, pp. 266, 1954.
- [32] P. C. Chow and L. Liu, "Relativistic Effects on the Electronic Band Structure of Compound Semiconductors" *Phys. Rev. Lett.*, vol. 140, pp. 1817-1826, 1965.
- [33] B. A. Bernevig and S. C. Zhang, "Quantum Spin Hall Effect", *Phys. Rev. Lett.*, vol. 96, pp. 106802, 2006
- [34] Y. Yao, F. Ye, X. L. Qi, S. C. Zhang, and Z. Fang, "Spin-orbit gap of graphene: First-principles calculations", *Physical Review B*, vol. 75, pp. 041401(1-4), 2007.
- [35] P. Esquinazi, D. Spemann, R. Hohn, A. Setzer, K. H. Han, and T. Butz "Induced Magnetic Ordering by Proton Irradiation in Graphite", *Phys. Rev. Lett.* vol. 91, pp. 227201, 2003.
- [36] O. V. Yazyev and L. Helm, "Defect-induced magnetism in graphene," *Phys. Rev. B*, vol. 75, pp. 125408, 2007.
- [37] J. J. Berzelius, "Thio and seleno compounds of the transition metals with the d⁰ configuration," *Ann. Phys. (Leipzig)* vol. 1, pp. 169, 1884.

- [38] Zhe Chuan Feng, in *SiC Power Materials: Devices and Applications*, edited by R. Hull, R. M. Osgood Jr, J. Parisi, and H. Warlimont (Springer-Verlag, Berlin, 2004).
- [39] H. J. Round, "Silicon Carbide Light-Emitting Diodes" *Electr. World*, vol. 19, pp. 309, 1907.
- [40] Y. M. Tairov and V. F. Tsvetkov, "Mechanisms of growth and defect properties of epitaxial SiC" *J. Cryst. Growth*, vol. 43, pp. 209, 1978.
- [41] S. Nishino, J. A. Powell, and H. A. Will, "Raman scattering studies of chemical-vapor deposited cubic SiC" *Appl. Phys. Lett.* vol. 42, pp. 460 (1983).
- [42] N. Kuroda, K. Shibahara, W. S. Yoo, S. Nishino, and H. Matsunami, *Ext. Abstr. 19th Conf. on Solid State Devices and Materials*, Tokyo, 227, 1987.
- [43] H. V. Jagodzinski, "SiC Materials and Devices" *Acta Cryst.* vol. 2, pp. 208, 1949.
- [44] F. Bechstedt and A. Belabbes, "Structure, energetics, and electronic states of III–V compound polytypes", *J. Phys.: Condens. Matter*, vol. 25, pp. 273201, 2013.
- [45] H. Deng, K. Endo and K. Yamamura, "Competition between surface modification and abrasive polishing: a method of controlling the surface atomic structure of 4H-SiC (0001)", *Nature*, vol. 5, pp. 8947, 2015.
- [46] Shaw, J. J. A. & Heine, V. "The nature of interplanar interactions in SiC polytypes" *J. Phys.: Condens. Mater.* vol. 2, pp. 4351–4361, 1990.
- [47] L. S. Ramsdell, "Studies on a Group of Silicon Carbide Structures" *Amer. Mineral.* 32, 64 (1947).
- [48] E. Bekaroglu, M. Topsakal, S. Cahangirov, and S. Ciraci, "A First-Principles Study of Defects and Adatoms in Silicon Carbide Honeycomb Structures", arXiv:1003.1318v1 [cond-mat.mtrl-sci] 5 Mar 2010.
- [49] Yoon Soo Park, in *SiC Materials and Devices*, edited by R. K. Willardson and E. R. Weber (Academic Press, USA, 1998).
- [50] A. Holmes, "principles of physical geology" Thomas Nelson and sons LTD, 1944.
- [51] M. W. Dashiell, L. V. Kulik, D. Hits, J. Kolodzey, and G. Watson. Carbon incorporation in $\text{Si}_{1-y}\text{C}_y$ alloys grown by molecular beam epitaxy using a single silicon-graphite source," *Applied Physics Letters*, vol. 72(7), pp. 833, 1998.

- [52] C. Y. Zhang, M. Yub, C. S. Jayanthib, S. Y. Wu and L. J. Zhou, “Shedding light on the self-assembly of stable SiC based cage nanostructures: A comprehensive molecular dynamics study”
- [53] C. Berger, Z. M. Song, X. B. Li, X. S. Wu, N. Brown, C. Naud, D. Mayou, T. B. Li, J. Hass, A. N. Marchenkov, E. H. Conrad, P. N. First and W. A. De Heer, “Electronic confinement and coherence in patterned epitaxial graphene.” *Science*, vol. 312, pp. 1191-1196, 2006.
- [54] K. S. Novoselov, A. K. Geim, S. V. Morozov, D. Jiang, M. I. Katsnelson, , I. V. Grigorieva, S. V. Dubonos and A. A. Firsov, “Two-dimensional gas of massless Dirac fermions in graphene,” *Nature*, vol. 438, pp. 197-200, 2005.
- [55] J. E. Field, “The mechanical and strength properties of diamond” , *Rep. Prog. Phys.* vol. 75, pp. 126505(35), 2012.
- [56] B. Feng, Z. Ding, S. Meng, Y. Yao, X. He, P. Cheng, L. Chen and and K. Wu, “Evidence of Silicene in Honeycomb Structures of Silicon on Ag(111)”, *Nano Lett.*, vol. 12 (7), pp. 3507–3511,2012.
- [57] Chen, S. J.; Liu, Y. C.; Shao, C. L.; Mu, R.; Lu, Y. M.; Zhang, J. Y.; Shen, D. Z.; Fan, X. W. *Adv. Mater.* vol. 17, pp. 586–590, 2005.
- [58] B.K. Kaushik and M.K. Majumder, “Carbon Nanotube: Properties and Applications” *Carbon Nanotube Based VLSI*,2015, DOI 10.1007/978-81-322-2047-3_2.
- [59] B. Aufray, A. Kara, S. Vizzini, H. Oughaddou, C. Léandri, B. Ealet, and G. Le Lay, “Graphene-like silicon nanoribbons on Ag(110): A possible formation of silicone” *Appl. Phys. Lett.* vol. 6, pp.183102, 2010.
- [60] L. J. Zhou, Y. F. Zhang, and L. M. Wu, “SiC₂ Siligraphene and Nanotubes: Novel Donor Materials in Excitonic Solar Cells”, *Nano Lett.* vol. 13, pp. 5431 –5436, 2013.
- [61] S. Cahangirov, M. Topsakal, E. Aktürk, H. Sahin, and S. Ciraci, “Two- and One Dimensional Honeycomb Structures of Silicon and Germanium” *Phys. Rev. Lett.* vol. 102, pp. 236804, 2009.
- [62] Z. Shi, Z. Zhang, A. Kutana and B. I. Yakobson, *ACS Nano*, 2015, DOI: 10.1021/acsnano.5b02753.
- [63] F. Banhart; J. Kotakoski, A. V. Krashennnikov, *ACS Nano*, vol. 5, pp. 26 –41, 2011.

- [64] X. Lin, S. Lin, Y. Xu, A. A. Hakro, T. Hasan, B. Zhang, B. Yu, J. Luo, E. Li and H. Chen, *J. Mater. Chem. C*, 2013, 1, 2131-2135.
- [65] Y. Li, F. Li, Z. Zhou and Z. Chen, *J. Am. Chem. Soc.*, 2010, 133, 900-908.
- [66] H. Dong, L. Zhou, T. Frauenheim, T. Hou, S. T. Leea and L. Youyong, "SiC7 siligraphene: a novel donor material with extraordinary sunlight absorption", *Nanoscale*, vol. 8, pp. 6994, 2016.
- [67] M. C. Payne, M. P. Teter, D. C. Allan, T. A. Arias and J. D. Joannopoulos, "Iterative minimization techniques for ab initio total-energy calculations: molecular dynamics and conjugate gradients" *Rev. Mod. Phys.* vol. 64, pp. 1045, 1991.
- [68] R. G. Parr and W. Yang, "Density-Functional Theory of Atoms and Molecules," New York: Oxford University Press. ISBN 0-19-509276-7, 1989.
- [69] P. Hohenberg and W. Kohn, "Inhomogeneous Electron Gas" *Phys. Rev. B*, vol. 136, pp. 684, 1964.
- [70] D.M. Ceperley and B.J Alder, "Ground State of the Electron Gas by a Stochastic Method" *Phys. Rev. Lett.* 45 566 (1980)
- [71] J. P. Perdew, K. Burke and M. Ernzerhof, "Generalized Gradient Approximation Made Simple" *Phys. Rev. Lett.* vol. 77, pp. 3865-3868, 1996.
- [72] W. Kohn and L. J. Sham, "Self-Consistent Equations Including Exchange and Correlation Effects" *Phys. Rev. A*, vol 140, pp. 1133, 1965.
- [73] D. Vanderbilt, "Soft self-consistent pseudo-potentials in a generalized eigenvalue formalism," *Phys. Rev. B*, vol. 41, pp. 7892-7897, 1990.
- [74] L. L. Foldy and S. A. Wouthuysen, "On the Dirac Theory of Spin 1/2 Particles and Its Non-Relativistic Limit" *Phys. Rev. B*, vol. 78, pp. 29, 1950.
- [75] K. Parlinski "Phonons calculated from first-principles", *EDP Sciences*, vol. 12, pp. 161–166, 2011.
- [76] A. Togo, I. Tanaka, "First principles phonon calculations in materials science," *Scr. Mater.* vol. 108, pp. 1–5, 2015.
- [77] P. Giannozzi, S. Baroni, N. Bonini, M. Calandra, R. Car, C. Cavazzoni, D. Ceresoli, G. Chiarotti, M. Cococcioni and I. Dabo, "Quantum ESPRESSO: a modular and open-

- source software project for quantum simulations of materials,” *J. Phys. Condens. Matter*, vol. 21, pp. 395502, 2009.
- [78] A. I. Khan, T. Chakraborty, N. Acharjee & S. Subrina, “Stanene-hexagonal boron nitride heterobilayer: Structure and characterization of electronic property” *Nature*, vol. 7, pp. 16347, 2017.
- [79] A. Kuc and T. Heine, “On the Stability and Electronic Structure of Transition-Metal Dichalcogenide Monolayer Alloys $\text{Mo}_{1-x}\text{X}_x\text{S}_{2-y}\text{Se}_y$ with $X = \text{W}, \text{Nb}$ ”, *Electronics*, vol. 5, pp. 1, 2016.
- [80] A. Hashimoto, K. Suenaga, A. Gloter, K. Urita, and S. Iijima, *Nature (London)*, vol. 430, pp. 870, 2004.
- [81] M. M. Ugeda, I. Brihuega, F. Guinea, and J. M. GómezRodríguez, *Phys. Rev. Lett.* vol. 104, pp. 096804, 2010.
- [82] N. Lu, H. Guo, W. Hu, X. Wu and X. C. Zeng, “Effects of line defects on the electronic properties of ZnO nanoribbons and sheets”, *J. Mater. Chem. C*, vol. 5, pp. 3121-3129, 2017.
- [83] L. Cai and C. Feng, “Effect of Vacancy Defects on the Electronic Structure and Optical Properties of GaN”, *Journal of Nanotechnology*, vol. 2017, pp. 6987430(6), 2017.
- [84] M. A. U. Absor, I. Santosa, Harsojo, and K. Abraha, “Defect-induced large spin-orbit splitting in the monolayer of PtSe_2 ”, arXiv:1708.06487v1 [cond-mat.str-el] 22 Aug 2017.

Appendix

Scf calculation of 2D-SiC

&CONTROL

```

calculation='scf', %Type of calculation
outdir='./rrr/', %The location name where we want to save data
prefix='unit_sic3', % Name of the compound or element
pseudo_dir='./C_Si/', %The directory where pseudopotential file stored
verbosity='low',
/

```

&SYSTEM

```

ibrav=4, What types of unit cell we will use. In this code hexagonal cell is used.
celldm(1)=5.72, celldm(3)=2.7259060621d0,
nat=2, % Number of atoms in the structure.
ntyp=2, % Types of atom used in the structure.
ecutwfc=30, % Cut off energy.
ecutrho=200,
input_dft='lda',
smearing='mv',
degauss=0.005d0,
occupations='smearing', % For Gaussian calculation
smearing='methfessel-paxton',
degauss=0.05,
/

```

&ELECTRONS

```

conv_thr=1d-06,
mixing_beta=0.7d0,
/

```

ATOMIC_SPECIES

```

C 12.010700d0 C.pz-van_ak.UPF
Si 28.085500d0 Si.pbe-n-van.UPF

```

ATOMIC_POSITIONS {crystal}

```

C 0.3333333333d0 0.1666666667d0 0.5000000000d0
Si 0.6666666667d0 0.8333333333d0 0.5000000000d0

```

K_POINTS {automatic}

```

12 12 1 0 0 0

```

%It means that it takes k point of $12 \times 12 \times 1$. 0 0 0 is whether to shift the mesh as a whole or not, in this case it is a mesh containing the Γ point. If it is 12 12 1 1 1 0, the Γ point will be at the center of the mesh.

List of Publications

Refereed Journal Papers

1. **Md. Rasidul Islam**, Md. Sherajul Islam, "Spin orbit coupling effects on the electronic structure of single layer two dimensional silicon carbide", Applied Physics Letter.(Under Review),2018.

Refereed International Conference Papers

1. **Md. Rasidul Islam**, Md. Masud Rana and A.S.M. Jannatul Islam “Electronic and Vibrational Properties of Single Layer Transition Metal Dichalcogenides (TMDC)” 2nd International Conference on Electrical & Electronic Engineering (ICEEE), 27-29 December 2017, RUET, Rajshahi, Bangladesh.
2. **Md. Rasidul Islam**, Md. Masud Rana and A.S.M. Jannatul Islam “ Effects of pseudopotential of electronic properties of two Dimensional SiC”, EECCMC 2018, International Conference on Electrical, Electronics, Computers, Communication, Mechanical and Computing (EECCMC-2018), Priyadarshini Engineering College, Chettiyappanur, Vaniyambadi - 635751, Vellore District, Tamil Nadu, India.
3. **Md. Rasidul Islam**, Md. Askarul Haque, Md. Fahim-Al Fattah, Md. Nur Kutubul Alam, Md. Rafiqul Islam “Dynamic Performance of Graphene Field Effect Transistor with contact Resistance” 5th International Conference on Informatics, electronics and vision (ICIEV-2016), Dhaka University, Dhaka, Bangladesh.
4. Md. Askarul Haque, **Md. Rasidul Islam**, Md. Nur Kutubul Alam, Md. Rafiqul Islam "Large Signal performance of Graphene-FET Considering Contact Resistance " 2nd International Conference on Electrical Information and Communication Technology(EICT 2015),KUET, Khulna, Bangladesh.
5. A.S.M. Jannatul Islam, **Md. Rasidul Islam**, Md. Sherajul Islam “Numerical Simulation of Vibrational Properties of AGNR with Vacancy and Stone wales Defects” 3rd International Conference on Electrical Information and Communication Technology(EICT 2015),KUET, Khulna, Bangladesh.
6. Md. Fahim-Al Fattah, Asif Abdullah Khan, **Md. Rasidul Islam**, Md. Ibne Sabid “Analysis on Band Structure and NEGF Approach for Graphene as a challenge material ” Proc. of 2nd International Conference on Electrical Engineering and Information & Communication Technology (ICEEICT 2015), Jahangirnagar University, Dhaka, Bangladesh, May 2015.
7. Abu Bakar Siddique, Alok Kumer Paul and **Md. Rasidul Islam** “Gold Coated Octagonal Photonic Crystal Fiber Biosensor using Surface Plasmon Resonance” International Conference on Electrical, Electronics, Computers, Communication, Mechanical and Computing (EECCMC-2018), Priyadarshini Engineering College, Chettiyappanur, Vaniyambadi - 635751, Vellore District, Tamil Nadu, India.